PAPER

Check for updates

Water soluble organometallic small molecules as promising antibacterial agents: synthesis, physical–chemical properties and biological evaluation to tackle bacterial infections†

Ines Bennour,[a] M. Núria Ramos,[b] Miquel Nuez-Martínez,[a]
Jewel Ann Maria Xavier, [ID][a] Ana B. Buades,[a] Reijo Sillanpää,[c] Francesc Teixidor, [ID][a]
Duane Choquesillo-Lazarte, [ID][d] Isabel Romero, [ID][e] Margarita Martinez-Medina[d]
and Clara Viñas [ID] *[a]

The Na[3,3′-Fe(8-I-1,2-C$_2$B$_9$H$_{10}$)$_2$] and Na[2,2′-M(1,7-C$_2$B$_9$H$_{11}$)] (M = Co^{3+}, Fe^{3+}) small molecules are synthesized and the X-ray structures of [(H$_3$O)(H$_2$O)$_5$][2,2′-Co(1,7-C$_2$B$_9$H$_{11}$)$_2$] and [Cs(MeCN)][8,8′-I$_2$-Fe(1,2 C$_2$B$_9$H$_{10}$)$_2$], both displaying a *transoid* conformation of the [M(C$_2$B$_9$)$_2$]$^-$ framework, are reported. Importantly, the supramolecular structure of [(H$_3$O)(H$_2$O)$_5$][2,2′-Co(1,7-C$_2$B$_9$H$_{11}$)$_2$] presents 2D layers leading to a lamellar arrangement of the anions while the cation layers form polymeric water rings made of six- and four-membered rings of water molecules connected *via* OH⋯H hydrogen bonds; B–H⋯O contacts connect the cationic and anionic layers. Herein, we highlight the influence of the ligand isomers (*ortho-/meta-*), the metal effect (Co^{3+}/Fe^{3+}) on the same isomer, as well as the influence of the presence of the iodine atoms on the physical–chemical and biological properties of these molecules as antimicrobial agents to tackle antibiotic-resistant bacteria, which were tested with four Gram-positive bacteria, five Gram-negative bacteria, and three *Candida albicans* strains that have been responsible for human infections. We have demonstrated an antimicrobial effect against *Candida* species (MIC of 2 and 3 nM for Na[3,3′-Co(8-I-1,2-C$_2$B$_9$H$_{10}$)$_2$] and Na[2,2′-Co (1,7-C$_2$B$_9$H$_{11}$)$_2$], respectively), and against Gram-positive and Gram-negative bacteria, including multiresistant MRSA strains (MIC of 6 nM for Na[3,3′-Co(8-I-1,2-C$_2$B$_9$H$_{10}$)$_2$]). The selectivity index for antimicrobial activity of Na[3,3′-Co(1,2-C$_2$B$_9$H$_{11}$)$_2$] and Na[3,3′-Co(8-I-1,2-C$_2$B$_9$H$_{10}$)$_2$] compounds is very high (165 and 1180, respectively), which reveals that these small anionic metallacarborane molecules may be useful to tackle antibiotic-resistant bacteria. Moreover, we have demonstrated that the outer membrane of Gram-negative bacteria constitutes an impermeable barrier for the majority of these compounds. Nonetheless, the addition of two iodine groups in the structure of the parent Na[3,3′-Co(1,2-C$_2$B$_9$H$_{11}$)$_2$] had an improved effect (3–7 times) against Gram-negative bacteria. Possibly the changes in their physical–chemical properties make the *meta*-isomers and the *ortho*-di-iodinated small molecules more permeable for crossing this barrier. It should be emphasized that the most active metallabis(dicarbollide) small molecules are both *transoid* conformers in contrast to the *ortho*- [3,3′-Co(1,2-C$_2$B$_9$H$_{11}$)$_2$]$^-$ that is *cisoid*. The fact that these small molecules cross the mammalian membrane and have antimicrobial properties but low toxicity for mammalian cells (high selectivity index, SI) represents a promising tool to treat infectious intracellular bacteria. Since there is an urgent need for antibiotic discovery and development, this study represents a relevant advance in the field.

[a]*Institut de Ciència de Materials de Barcelona, Consejo Superior de Investigaciones Científicas, Campus Universitat Autònoma de Barcelona, 08193 Bellaterra, Spain. E-mail: clara@icmab.es; Fax: +34-935805729*
[b]*Microbiology of Intestinal Diseases, Biology Department, Universitat de Girona, 17003 Girona, Spain*
[c]*Dept. of Chemistry, University of Jyväskylä. FIN-40014, Jyvaskyla, Finland*
[d]*Laboratorio de Estudios Cristalográficos, IACT, CSIC-Universidad de Granada, Armilla, 18100 Granada, Spain*
[e]*Departament de Quimica and Serveis Tècnics de Recerca, Universitat de Girona, C/M. Aurèlia Campmany, 69, E-17003 Girona, Spain*

Introduction

Over the years, the rapid development and spread of new antimicrobial resistance (AMR) has forced the World Health Organization (WHO) to recognize it is a major risk to public health.[1] AMR has made many antimicrobials ineffective in treating clinically ill patients. Even medical procedures such as major surgery, organ transplantation, and cancer chemotherapy have become very risky in the absence of effective antimicrobials for the prevention and treatment of nosocomial infections. It is estimated that nosocomial infections affect around 4.1 million people in the European Union each year, being around the 7%–8% of patients receiving healthcare in Spain.[2] The leading cause of nosocomial infections throughout the world is the ESKAPE pathogens (*Enterococcus faecium*, *Staphylococcus aureus*, *Klebsiella pneumoniae*, *Acinetobacter baumannii*, *Pseudomonas aeruginosa*, and *Enterobacter* species), most of them being multidrug-resistant isolates.[3] Because of the drastic rise in antibiotic resistance, greater than the discovery of new antibiotics, there is an urgent need for the development and evaluation of novel effective antimicrobial agents active against drug-resistant forms.

Nanomaterials, owing to their high specific surface area and abundant modification sites, have been shown to be promising weapons for cancer therapy[4] and to possess a great potential as new antimicrobial agents effective against resistant bacteria.[5] Recent reviews update the advances in nanoparticles[6] and metal complexes[7] as emerging antibacterial nanomedicine for enhanced antibiotic therapy.

Most of the marketed small molecules[8] are organic molecules, which incorporate nitrogen, oxygen, and halogens besides carbon and hydrogen, all of them the right-hand neighbors of carbon. Boron is an element which, despite being located on the left side of carbon in the Periodic Table, has the property to build molecules by covalent self-bonding.[9] The neutral twelve-vertex icosahedral *closo*-carboranes $C_2B_{10}H_{12}$, *ortho*-, *meta*-, or *para*-isomers, the anionic *nido*-carboranes and the anionic metallabis(dicarbollides) $[M(C_2B_9H_{11})_2]^-$ (M = Co^{3+}, Fe^{3+}) (Fig. 1) rank among the most chemically and biologically stable small molecular compounds known.[10–12]

The most studied of the metallabis(dicarbollides) is [3,3′-Co(1,2-$C_2B_9H_{11})_2]^-$ anion, [**1**]$^-$. Prominent features of the [**1**]$^-$ anion are 3D aromaticity,[10,13] thermal, chemical (withstanding strong acid, moderate base, high temperatures and intense radiation)[14] and biological (neither degradation nor chemical modification compounds were identify after cell uptake) stability,[15,16] and solubility in both polar and nonpolar solvents.[11] Besides these, other characteristic properties of this anion are: (i) the negative charge of [**1**]$^-$ is spread all over the molecule,[10,17] (ii) [**1**]$^-$ aggregates in *cisoid* conformation in aqueous solution by means of B–H⋯H–$C_{cluster}$ dihydrogen bond formation,[18] and (iii) although lacking the classical hydrophilic–hydrophobic structure,[19] [**1**]$^-$ shows amphiphilic behavior,[20] which was experimentally proved by a study based on the electrolysis of water.[21] Furthermore, the anion [**1**]$^-$, the 3D shape of which is reminiscent of the Greek letter θ and has a size of 1.1 nm × 0.6 nm, produces strong dihydrogen-bond B–H⋯H–N interactions with the amine groups of amino acids[22] and proteins.[23] Moreover, [**1**]$^-$, which can cross through synthetic lipid membranes without disrupting membrane integrity,[24] displays low toxicity *in vitro*[15,16] and
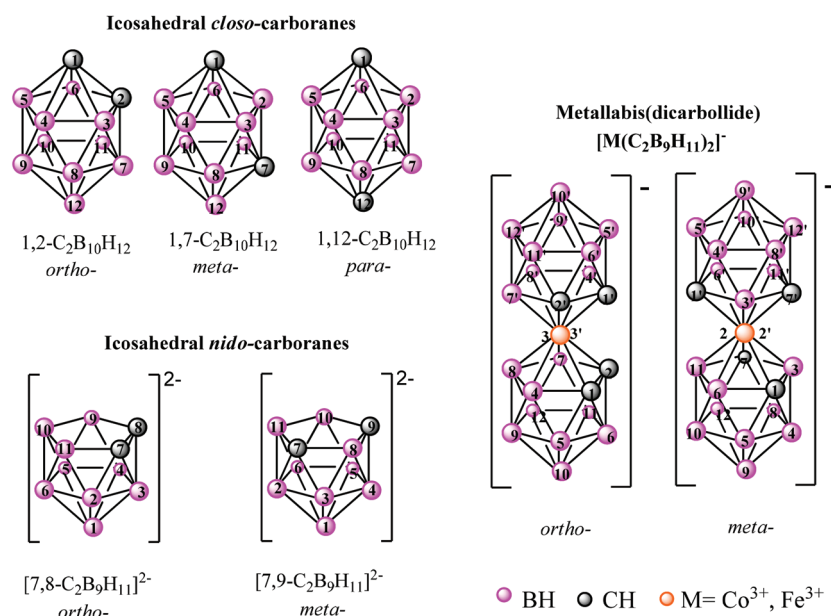
Fig. 1 The numbering of the *closo*-$C_2B_{10}H_{12}$ clusters, their *nido*-$[C_2B_9H_{11}]^{2-}$ ligands as well as the metallabis(dicarbollide) $[M(C_2B_9H_{11})_2]^-$ platforms. Circles in grey represent the C_c–H vertices, the orange ones correspond to metal (M = Co^{3+}, Fe^{3+}) while the circles in pink correspond to B–H vertices.

in vivo[16,25] and high uptake by relevant cancer cells,[15,26] accumulating *in vitro* within the nuclei of living cells.[16] Additionally, the anionic $[M(C_2B_9H_{11})_2]^-$ clusters can be modified at the different vertexes by halogenation,[27–29] and are responsible for additional physicochemical properties.[10,29,30] Recently, amphiphilic inorganic anionic [**1**]$^-$ clusters have been proposed to stabilize oil-in-water nanoemulsions of poorly water soluble drugs.[31] The increasing evidence that boron cluster compounds are promising antimicrobial agents has been reviewed recently.[32]

There are two groups of oral antibacterial agent on the market, all of them small organic molecules: one comprises molecules in the molecular weight range of 340–450 Da and the other molecules of 700–900 Da.[33] Following our studies on metallacarboranes in medicinal chemistry,[34] we report herein high-yield syntheses of the sodium salts of four isomeric pristine metallabis(dicarbollide) molecules (321–324 Da) and their di-iodinated derivatives (572–576 Da) as abiotic, small, purely inorganic molecules for antimicrobial therapy. Chart 1 displays the general schematic representation of all the small inorganic anionic $[M(C_2B_9H_{11-n}X_n)_2]^-$, (M = Co^{3+}, Fe^{3+}, n = 1, X = H or I), molecules studied in this paper as antimicrobial agents.

ortho-Isomers are: Na[3,3′-M(1,2-$C_2B_9H_{11}$)$_2$], M = Co, Na[**1**]; Fe, Na[**2**]. Na[3,3′-M(8-I-1,2-$C_2B_9H_{10}$)$_2$], M = Co, Na[**3**]; Fe, Na [**4**]. *meta*-Isomers are: Na[2,2′-Co(1,7-$C_2B_9H_{11}$)$_2$], M = Co, Na[**5**]; Fe, Na[**6**].

Herein, we highlight the effect of the ligand isomers (*ortho*-/*meta*-), the metal effect (Co^{3+}/Fe^{3+}) on the same isomer as well as the influence of the presence of iodine atoms on the physical and chemical properties of these small inorganic

anionic molecules with activity against four Gram-positive bacteria, five Gram-negative bacteria, and three *Candida albicans* strains that have been responsible for human infections. A structure–activity relationship has been proposed, which clearly supports the antimicrobial activity of these pristine metallabis(dicarbollide) complexes.

Results and discussion

The synthesis of the small anionic sandwich metallabis(dicarbollides) is achieved by a metal complexation reaction of the *nido*-[$C_2B_9H_{11}$]$^{2-}$ ligands in several conditions (see scheme S1–S4 in the ESI†).[35] There are two positional isomers of the *nido* [$C_2B_9H_{11}$]$^{2-}$ carboranyl ligands (Fig. 2a): the isomer *ortho*-([7,8-$C_2B_9H_{11}$]$^{2-}$) in which the two carbon atoms are connected and, the isomer *meta*-([7,9-$C_2B_9H_{11}$]$^{2-}$) wherein a boron atom is located in between the two carbon atoms in the $\eta^5C_2B_3$ coordinating face. Depending on the starting [$C_2B_9H_{11}$]$^{2-}$ *nido* carboranyl ligand, two positional *ortho*- and *meta*-metallabis (dicarbollide) isomers are obtained, whose empirical formulae are [3,3′-M(1,2-$C_2B_9H_{11}$)$_2$]$^-$ and [2,2′-M(1,7-$C_2B_9H_{11}$)$_2$]$^-$, (M = Co^{3+}, Fe^{3+}), respectively (Fig. 2). Fig. 1 displays the numbering of these two platforms.

The four anionic *ortho*- and *meta*-metallabis(dicarbollide) isomers are abbreviated as [**1**]$^-$, [**2**]$^-$, [**5**]$^-$ and [**6**]$^-$ for M = Co^{3+} and Fe^{3+}, respectively. As shown in Fig. 2, five different conformations that provide a different dipole moment[36] can be found for the *ortho*-metallabis(dicarbollide) isomer: *cisoid*-1, *gauche*-1, *transoid*, *gauche*-2 and *cisoid*-2 (being *cisoid*-1 and *cisoid*-2 as well as *gauche*-1 and *gauche*-2 equivalent), while
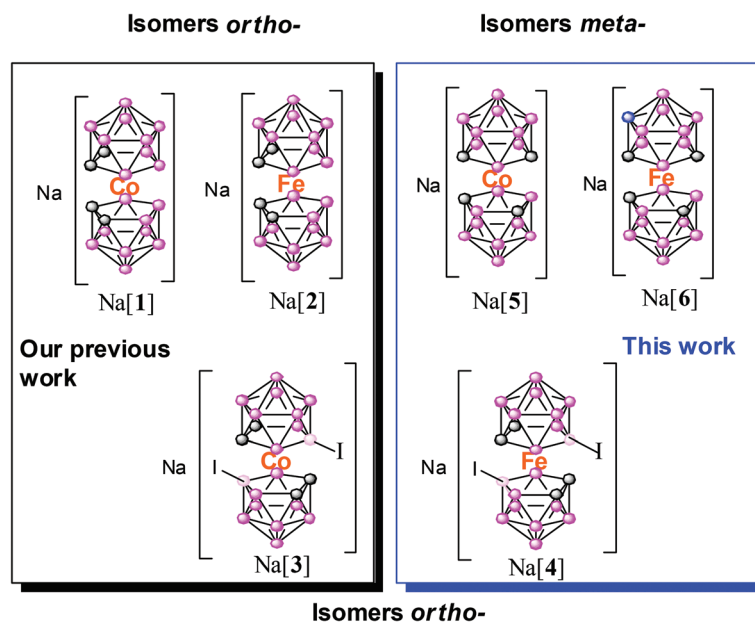
Chart 1 Schematic representation of the metallabis(dicarbollide) complexes studied and their abbreviation. Circles in grey represent the C_c−H vertices, the orange ones correspond to metal (M = Co^{3+}, Fe^{3+}) while the circles in light and dark pink correspond to B−H and B−I vertices, respectively.

a)   b)
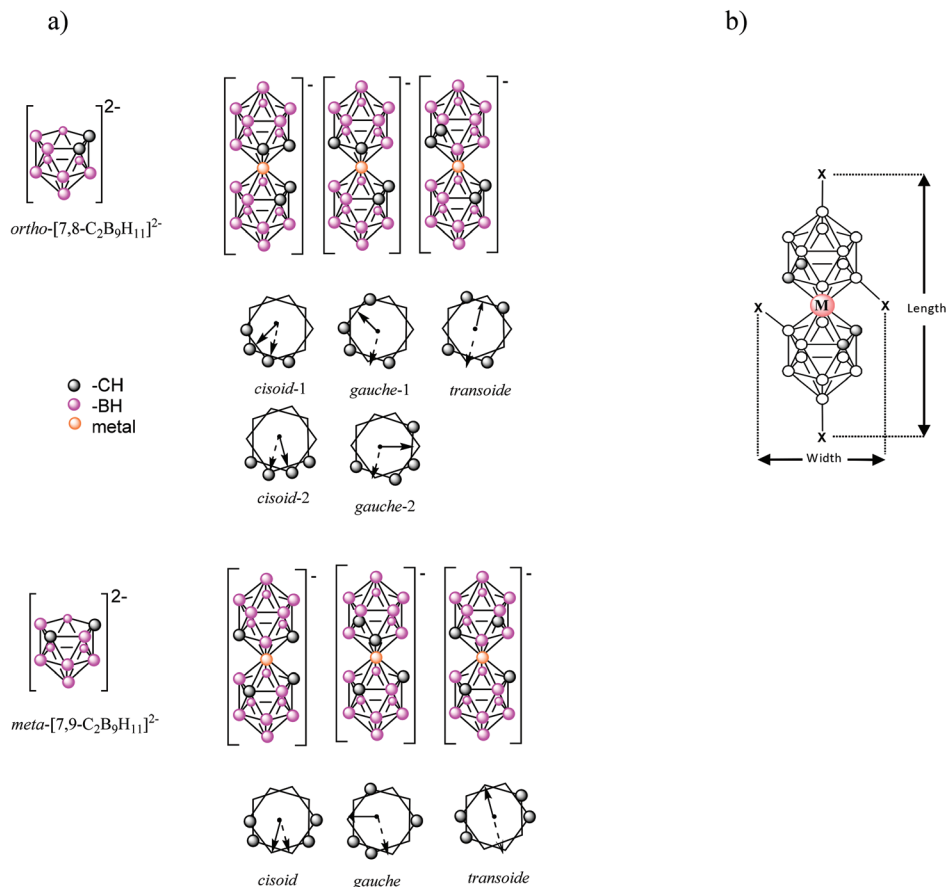
Fig. 2 (a) Schematic representation of the icosahedral *ortho*- and *meta-nido*-[C$_2$B$_9$H$_{11}$]$^{2-}$ η^5 ligands and the anionic *ortho*- and *meta*-metallabis (dicarbollide) [M(C$_2$B$_9$H$_{11}$)$_2$]$^-$ isomers and their conformers (the arrows indicate the direction of the dipole moments of the compounds). (b) The graphical definition of length and width concepts for the small [M(C$_2$B$_9$H$_{11-n}$X$_n$)$_2$]$^-$, (M = Co^{3+}, Fe^{3+}, *n* = 1, X = H or I), anionic molecules. Circles in grey represent the C$_c$–H vertices, the orange ones correspond to metal (M = Co^{3+}, Fe^{3+}) while the circles in pink correspond to B−H vertices.

three different conformations are found for the *meta*-metalla-bis(dicarbollide) isomer.

The sodium salts of [**1**]$^-$, [**2**]$^-$ and [**3**]$^-$ were synthesized as previously reported by us (see Schemes S1–S3 in the ESI†).[18,37] The new Na[**5**] and Na[**6**] species have been obtained in this article by means of a cationic exchange resin of the corresponding tetramethyl ammonium or cesium salts and are fully characterized by spectroscopic techniques IR, ^{1}H, ^{1}H{^{11}B}, ^{11}B and ^{11}B{^{1}H} NMR, MALDI-TOF-MS, UV-vis, cyclic voltammetry (CV) as well as by thermal analysis (TGA/DSC) as stated at the Experimental section and ESI.†

Despite multiple attempts, no good crystals of Na[**5**] suitable for X-ray diffraction studies, to compare with the reported Na[**1**], could be obtained,[38] but suitable crystals of the protonated salt of [**5**]$^-$ were obtained from aqueous solution (Fig. 3).

The Cs[3,3′-Fe(8-I-1,2-C$_2$B$_9$H$_{10}$)$_2$], Cs[**4**], was synthesized in this article from [**2**]$^-$ and *N*-iodosuccinamide by a modification of the original synthesis by Kazheva *et al.*[39] This procedure permits the isolation of Cs[**4**] with an easy purification step. Crystals of Cs[**4**] were grown from an acetonitrile solution (Fig. 4). The corresponding water soluble small molecule Na[**4**]

was obtained from the Cs[**4**] salt by means of cationic exchange resin (Scheme 1).

Crystal structures of H[5] and Cs[4]

An examination of the Cambridge Structural Database[40] showed one hit for the diamagnetic Co^{3+} unsubstituted parent [**5**]$^-$,[35e] and one for the paramagnetic [**4**]$^-$ framework.[39] The CDS refcodes are HODGAL (*transoid* rotamer),[35e] and GANQIY (*transoid* rotamer),[39] respectively. It is to be noted that none of the reported crystal structures of the *ortho*- and *meta*-parent metallabis(dicarbollide) frameworks contain a proton as counter ion. The volume (286.5 Å^3) and molecular shape (cylindrical with one of the moments larger than the other two) of the [**2**]$^-$ anion was determined by Mingos *et al.* using the VOLUME program.[41]

Crystal structure of H[5]. Suitable crystals for X-ray diffraction of the protonated salt of monoanionic [**5**]$^-$ were obtained from aqueous solution by slow evaporation. The crystal structure of H[**5**], [(H$_3$O)(H$_2$O)$_5$][2,2′-Co(1,7-C$_2$B$_9$H$_{11}$)$_2$], is displayed in Fig. 3. The anionic moiety (Fig. 3a) presents a *transoid* conformation and its B–Co, C–Co, C–B and B–B bond parameters
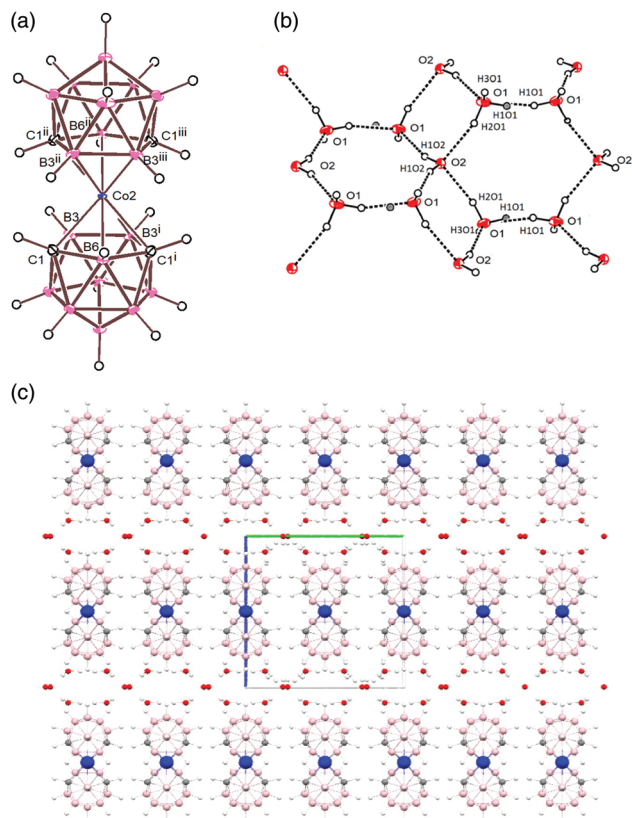
Fig. 3 (a) The anionic unit of the salt [(H$_3$O)(H$_2$O)$_5$][2,2′-Co(1,7-C$_2$B$_9$H$_{11}$)$_2$]] and (b) the hydrogen bond system for the [(H$_3$O)(H$_2$O)$_5$]$^+$ cation. The population parameter for H1O1 is 0.5, which means that only black or white H1O1's are present at the same time in the six-member water ring parts of [(H$_3$O)(H$_2$O)$_5$][2,2′-Co(1,7-C$_2$B$_9$H$_{11}$)$_2$]. (c) Part of the crystal structure of the [(H$_3$O)(H$_2$O)$_5$][5] compound viewed along the a axis.

are very similar to those for HODGAL.[35e] The cationic part is formed of polymeric water rings (Fig. 3b), which are made of six- and four-membered rings of water molecules. The rings

are held together *via* OH···O hydrogen bonds. The O···O distances are from 2.725 to 2.785 Å. The protons in these cationic layers are located on the O1 atoms at the H1O1 positions with a total population parameter of 1 (0.25 at each four O1 atoms). The water layers have weak B–H···O contacts (B–H5···O2 = 2.671 Å and B–H8···O1 = 2.879 Å), which assist the connection of the cationic and anionic parts (Fig. 3c).

Crystal structure of Cs[4]. A survey in the CSD (version 5.41, update August) reveals that only two crystal structures containing the 8,8′-diiodo derivative of metallabis(dicarbollide) anion have been reported: an iron complex anion [4]$^-$ with a bis(ethylenedithio)tetrathiafulvalene cation (refcode GANQIY)[39] and a cobalt complex anion [3]$^-$ with a Cs$^+$ (refcode DEXPIF).[42] Compound Cs[4] is actually [Cs(MeCN)][4] and crystallizes in the monoclinic C2/c space group. The presence of an acetonitrile molecule in the structure of the Fe complex results in the compounds Cs[4] and Cs[3] being not isostructural. The asymmetric unit of [Cs(MeCN)][4] consists of a half-anionic complex unit, with the iron and the cesium ions occupying an inversion center, and a half acetonitrile molecule at a 2-fold axis. The [4]$^-$ anion has a *transoid* rotamer and bonds *via* I-atoms to two Cs$^+$ ions (Cs–I distances of 3.8737(3) Å) (Fig. 4).

The acetonitrile molecule forms a bridge between Cs$^+$ ions, which form linear chains (Fig. 5) along the c axis (Cs–N distances 3.137(5) Å; Cs···Cs distances 4.46005(15) Å). The Cs cation has a coordination number of 8: two I, two N, two H from B9 with Cs–H distances of 3.147 Å, and two H from B12 with Cs–H distances of 3.280 Å. The linear Cs chains results in a body center type structure in which the Cs···Cs chain distances are 12.514 and 12.642 Å, thus generating a supramolecular structure showing alternating layers of iron complex anions and Cs$^+$ cations plus acetonitrile solvent molecules stacked along the a axis.

Both related cobalt and iron complexes Cs[3] and Cs[4] exhibit similar packing indexes (0.726 and 0.725, respectively). Nonetheless, the distances observed for Cs···Cs and Cs···I interactions are shorter in [Cs(MeCN)][4] than in the analogue
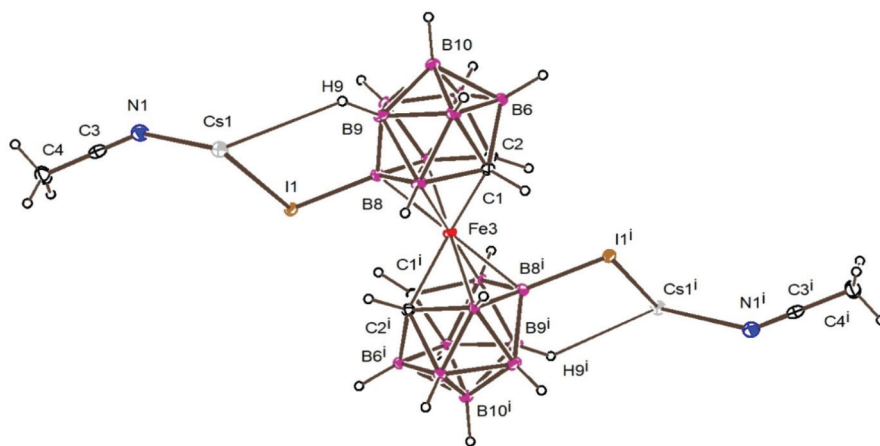
Fig. 4 Molecular unit of Cs[4] with atom labelling showing thermal ellipsoids at the 30% probability level. Symmetry operation i = −x + $\frac{1}{2}$, −y + 1$\frac{1}{2}$, 1 − z. The Cs1−N1, Cs1−I1 and Cs1−H9 distances are 3.8737(3), 3.137(5) and 3.280 Å, respectively.
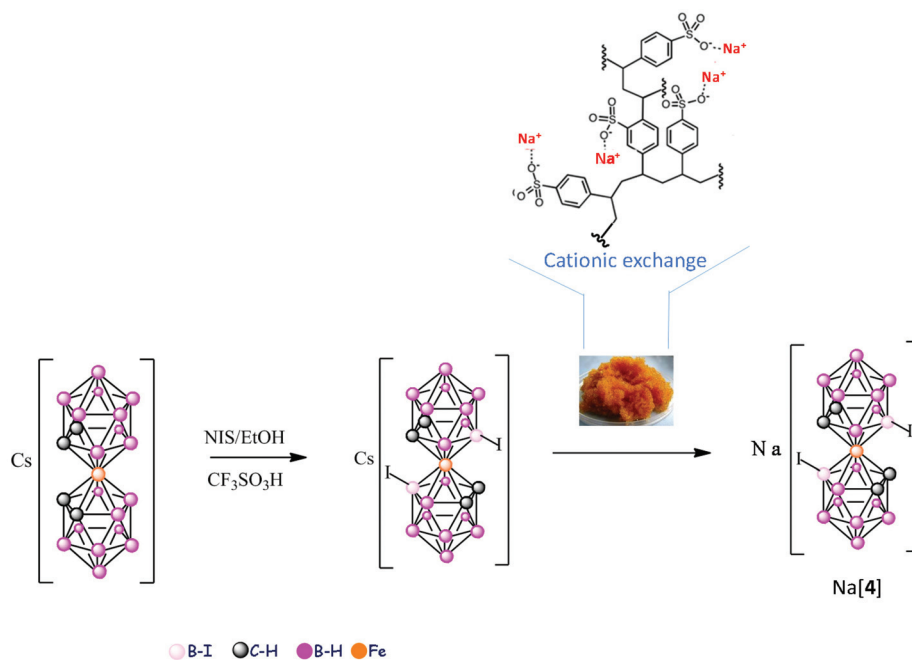
Scheme 1 Synthesis of the cesium salt of the anionic [**4**]⁻ small molecule by using NIS in EtOH, and its sodium salts by cation exchange resin. Circles in grey represent the C_c−H vertices, the orange ones correspond to Fe^{3+} while the circles in dark and light pink correspond to the B−H and B−I vertices, respectively.

Cs[**3**] (Cs···Cs distance 6.813 Å and Cs···I distance 4.140 Å), which can be attributed to the acetonitrile solvent in the crystal packing.

Physico-chemical properties of metallabis(dicarbollides) and their di-iodinated derivatives

As mentioned in the introduction, there are several published studies on the properties of [**1**]⁻ but, to the best of our knowledge, studies pertaining to [**2**]⁻, [**5**]⁻ and [**6**]⁻ are scarce. Herein, we report on the physico-chemical, spectroscopic, and electrochemical studies of these less-known small inorganic molecules. The different behavior of me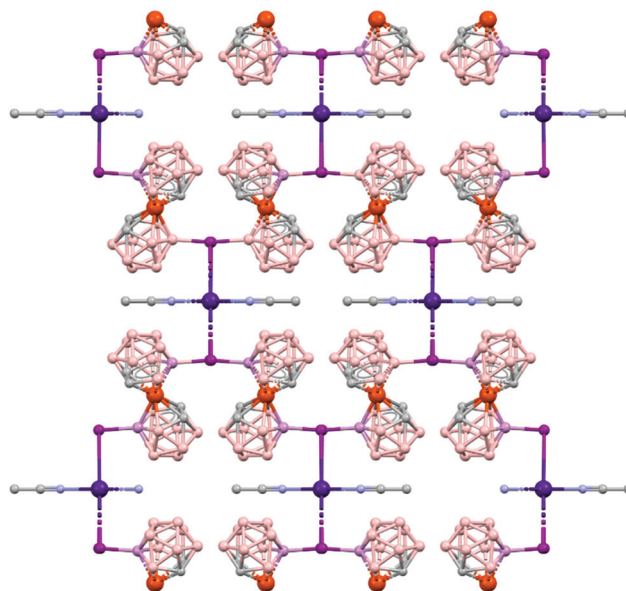tallabis(dicarbollide) isomers (*ortho/meta*) in aqueous solution have been studied by dynamic light scattering (DLS), and transmission electron microscopy (TEM and CryoTEM).

Dynamic light scattering (DLS) and transmission electron microscopy (TEM). It has been reported that anionic [3,3′-Co $(X_3$-1,2-$C_2B_9H_8)_2$]⁻, X = H, Cl, Br, Me, derivatives behave similarly to a surfactant in aqueous solutions[43] and that [*o*-COSAN]⁻ can self-assemble in spherical aggregates with a radius of around 100 nm in a fairly monodisperse way, depending on the concentration and aging of the solutions.[20]

In medicinal chemistry, it is crucial to know the compounds' behavior in aqueous solution. Hence, we performed dynamic light scattering of the less studied metallabis(dicarbollides), Na[**2**], Na[**4**], Na[**5**], and Na[**6**] in aqueous solutions at different concentrations to obtain information on their possible self-assembly. Fig. 6 displays the DLS measurements in aqueous solution of the reported small ferrabis(dicarbol-

Fig. 5 Part of the crystal structure of compound Cs[**4**], viewed along the *c* axis. Hydrogen atoms are omitted for clarity. Circles in purple correspond to I atoms, the dark blue the Cs⁺, the light blue the N atoms, the grey represent the C_c−H vertices, the orange ones correspond to Fe^{3+} metal while the circles in light and dark pink correspond to the B−H and B vertices, respectively.

lide) anionic molecules as well as the previously reported Na[**1**][18] for comparison. A decrease in the hydrodynamic diameter of the aggregates was observed when the concentration increased. At a concentration of 50 mM, a change in aggregate
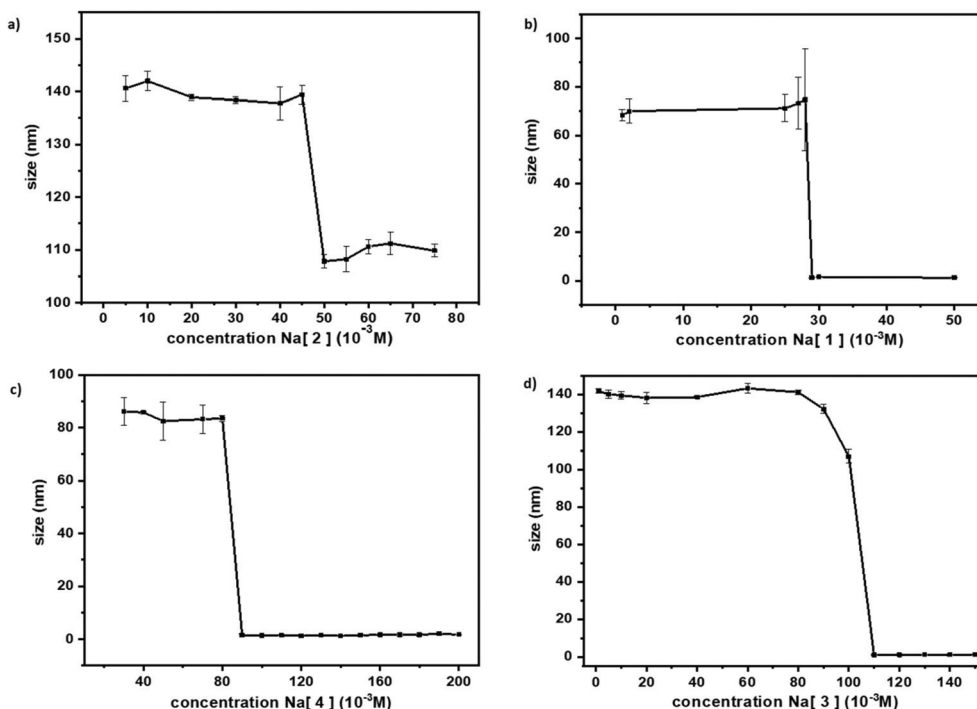
Fig. 6 DLS studies of (a) Na[**2**]: concentration range 5–75 mM; (b) Na[**1**]: concentration range 1–50 mM; (c) Na[**4**]: concentration range 5–200 mM; and (d) Na[**5**]: concentration range 5–150 mM in aqueous solution.

size was observed for Na[**2**] from 140 nm to 108 nm. For the iodinated derivative, Na[**4**], the change in size was observed at 90 mM and was from 83.5 nm to 1.5 nm. In all four *ortho*-metallabis(dicarbollide) isomers (Fig. 6), a decrease in the hydrodynamic diameter of the aggregates was observed by DLS experiments when the concentration was increased, which could be attributed to a Coulomb explosion of the closely packed monolayer aggregates into small micelles. The aggregate size of Na[**3**] at 110 mM changes from 1.11 nm to 110 nm at 107 mM.[44]

In order to visualize the large and small aggregates of ferra-bis(dicarbollides) TEM images were taken. In the case of the parent Na[**2**], CryoTEM and TEM images of 1 mM aqueous solution were obtained for comparison (Fig. 7).

In the case of the *meta* isomers, Na[**5**] and Na[**6**], no aggregates were observed by DLS measurements in the concentration range 120 – 1 mM and 110 – 1 mM respectively, which is in agreement with the dynamic $^1H\{^{11}B\}$ NMR study (ESI†). To summarize, the Na[**1**] and Na[**5**] isomers behave differently in aqueous solution: the *ortho*-isomer forms aggregates while the latter do not.
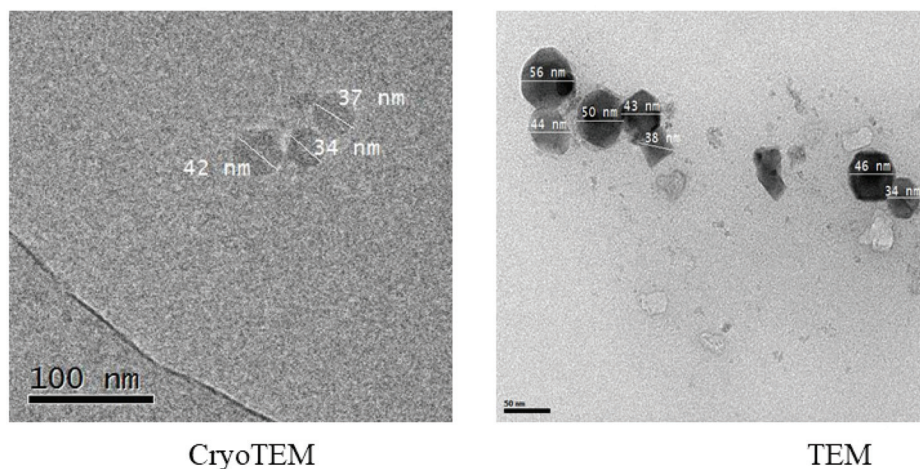
Fig. 7 CryoTEM and TEM images of an aqueous solution 1 mM of Na[**2**]. Bar length is 100 nm in the CryoTEM and 50 nm in the TEM.

Cyclic voltammetry studies. The central core of the metalla-bis(dicarbollide) anions, "$M(C_2B_3)_2$", displays a reversible electrochemical behaviour similar to the core of ferrocene, "$Fe(C_5)_2$".[45] Only one coupled reduction/oxidation process in the range of potentials studied (−2.20 to +0.50 V referenced to ferrocene (F_c^+/F_c) that was taken as zero) were observed for the reported sodium salt of all metallabis(dicarbollide) complexes. The cathodic current is caused by the reduction of either $Co^{3+} \rightarrow Co^{2+}$ or $Fe^{3+} \rightarrow Fe^{2+}$, and the reverse oxidation process is also observed; a point to be noted is that both partners are negatively charged. Fig. 8 shows the cyclic voltammograms of the four *ortho*- and *meta*-sandwich $[M(C_2B_9H_{11})_2]^-$ (M = Co, Fe) complexes as well as their $[8,8'-I_2-M(C_2B_9H_{11})_2]^-$ (M = Co^{3+}, Fe^{3+}) derivatives. A conceivable further 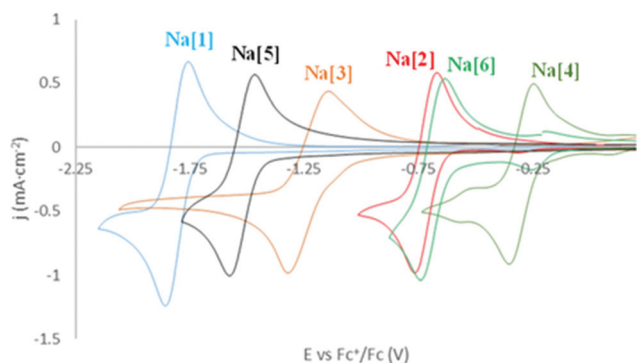reduction process $Co^{2+} \rightarrow Co^+$ or $Fe^{2+} \rightarrow Fe^+$ was not observed in the range of electrode potentials investigated.

Table 1 summarizes the redox potential E_{red}, ΔE values ($\Delta E = E_{red} - E_{ox}$) and $E_{1/2}$ ($E_{1/2} = (E_{red} + E_{ox})/2$) of all the redox couples related to F_c^+/F_c. $E_{1/2}$ is the half wave potential associ-

ated with the reversible redox Co^{3+}/Co^{2+} process. We observed that the $E_{1/2}$ potential of the studied anionic charged metallabis(dicarbollide) complexes can be tuned by changing the metal, changing the positional isomer of the ligands or by introducing an iodo substituent on the pentagonal coordinating η^5-C_2B_3 face of the ligands. By changing the metal, the $E_{1/2}$ potential decreases +1.1 V from $[1]^-$ to $[2]^-$ (−1.81 V to −0.73 V, respectively) and the same tendency is observed in the two redox couples $[3]^-$ to $[4]^-$ (−1.33 V to −0.36 V, respectively).

A small variation in the $E_{1/2}$ potential is observed between the isomers $[1]^-$ and $[5]^-$ (−1.81 V to 1.55 V, respectively) as well as when comparing $[2]^-$ with $[6]^-$ (−0.73 V to −0.79 V, respectively), while in $[3]^-$ and $[4]^-$, the presence of two iodo groups at the B(8,8′) positions at the η^5-C_2B_3 face of either $[1]^-$ or $[2]^-$ decreases the $E_{1/2}$ potential +0.48 V and +0.37 V, respectively.

UV-visible studies. The six metallabis(dicarbollide) small molecules show absorption bands in the UV-vis region as shown in Fig. 9. The visible spectrum of $[1]^-$ in methanol reported by Hawthorne *et al.* consists of four absorptions at 216, 293, 345, and 445 nm,[35c] which agrees with the one absorption band at 287 nm reported previously.[28b]

Table 2 displays the UV-vis spectra of the studied $[M(C_2B_9H_{11})_2]^-$ complexes in water. λ positions and ε values are reported and were calculated following line fitting analysis.

The compounds exhibit intense bands around 270–280 nm, and in the case of Na[**3**] a weak band is also observed at 331 nm. These intense bands have been assigned to charge transfer from the ligand framework towards the metal centre (LMCT).[47]

The presence of cobalt in the metallacarborane produces a bathochromic shift of the absorptions *versus* iron, and lower wavelengths have been observed for the Fe compounds in comparison with the Co ones. The UV-vis spectra do not seem to be affected by the different isomers *ortho*- and *meta*- in the case of cobaltabis(dicarbollide) compounds Na[**1**] and Na[**5**] (λ = 280 nm). However, an increase in wavelength takes place for the *meta*-isomer in the case of Na[**6**] (λ = 278.5 nm) in comparison with the *ortho*-isomer Na[**2**] (λ = 271 nm). For the iodo-derivatives, Na[**3**] and Na[**4**], a shift to the visible spectrum, was observed (λ = 286.5 and λ = 285.5 nm) with respect to the corresponding unsubstituted metallacarboranes Na[*o*-COSAN] and Na[*o*-FESAN] (λ = 280 and λ = 271 nm), respectively. A similar behavior has been observed for the dichloro-derivatives, although in the latter the bathochromic shift, caused by the chlorine substituents, is greater.[28b]

Solubility and lipophilicity. The aqueous solubility of a compound (S or log S), which is the concentration (mol L^{-1}) of its saturated aqueous solution, is an important factor that affects its bioavailability.[48] There are several factors affecting the solubility of a compound such as the size and shape of the molecule, its polarity and hydrophobicity, as well as its ability to participate in intra- and intermolecular hydrogen or dihydrogen bonding. Taking advantage of the fact that *meta*-metallabis(dicarbollide) small molecules absorb at the UV-vis region, we used a quantitative method based on UV-vis spectroscopy

Fig. 8 Cyclic voltammogram responses of 5 mM solution of the *ortho*- and *meta*-sandwich $[M(C_2B_9H_{11})_2]^-$ and the di-iodinated $[M(8,8'-I-o-$metallabis(dicarbollide)$)]^-$ (M = Co, Fe) complexes recorded at a glassy carbon electrode in dry CH_3CN using $[NnBu_4][PCl_6]$ (0.1 M) as the supporting electrolyte, referenced to ferrocene (F_c^+/F_c).

Table 1 Reduction potentials E_{red}, ΔE values ($\Delta E = E_{red} - E_{ox}$) and $E_{1/2}$ ($E_{1/2} = (E_{red} + E_{ox})/2$) obtained from the cyclic voltammetry studies in acetonitrile. The F_c^+/F_c couple is taken as the zero reference

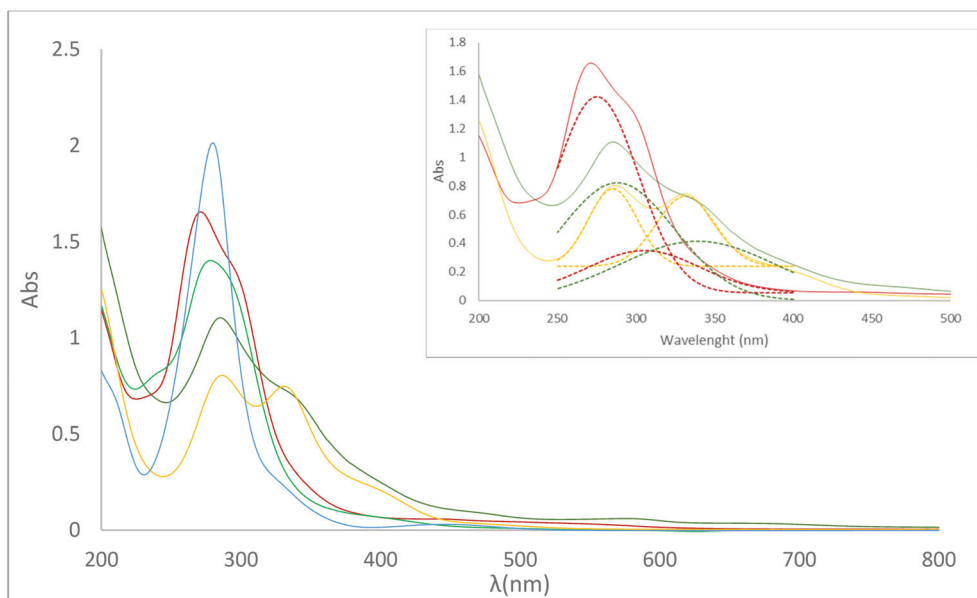| Metal	Complex	$E_{1/2}$ (V)	ΔE (V)	E_{red} (V)
Co^{3+}/Co^{2+}	Na[**1**]	−1.81 (ref. 46)	0.10	−1.86
	Na[**5**]	−1.55	0.12	−1.60
	Na[**3**]	−1.33 (ref. 46)	0.19	−1.42
Co^{4+}/Co^{3+}	Na[**1**]$^-$	1.16	0.09	1.12
	Na[**5**]	1.44	0.10	1.38
	Na[**3**]	1.07	0.23	0.95
Fe^{3+}/Fe^{2+}	Na[**2**]	−0.73	0.10	−0.78
	Na[**6**]	−0.79	0.11	−0.85
	Na[**4**]	−0.36	0.10	−0.41
Fe^{4+}/Fe^{3+}	Na[**2**]	0.75	0.16	0.67
	Na[**6**]	0.66	0.10	0.61
	Na[**4**]	1.11	0.14	1.04

Paper

Fig. 9 UV-visible spectra of the metallabis(dicarbollides) in 0.08 mM aqueous solution. Na[**1**] in blue, Na[**3**] in yellow, Na[**5**] in black, Na[**2**] in red, Na[**4**] in dark green, Na[**6**] in light green. Inset: de-convoluted peaks of Na[**2**], Na[**4**] and Na[**3**] in their respective dashed colours.

Table 2 UV-Visible spectra of the studied $[M(C_2B_9H_{11})_2]^-$ complexes in 0.08 mM aqueous solution

Complex	Max λ (0.08 mM)	Abs (0.08 mM)	ε (L mmol^{-1} cm^{-1})
Na[**4**]	333.5	0.720	9.000
	285.5	1.104	13.80
Na[**2**]	302.5	1.217	15.21
	271	1.665	20.81
Na[**6**]	278.5	1.401	17.51
Na[**3**]	331	0.747	9.338
	286.5	0.804	10.05
Na[**1**]	280	2.013	25.16
Na[**5**]	280	2.247	28.08

to calculate the log S of the two *meta*- metallabis(dicarbollide) small molecules, whose values are shown in Table 3. In this method, the UV-vis absorption of the aqueous solution containing the metallabis(dicarbollide) was measured to study its molar absorptivity (ε_{max}); as this is proportional to the concentration of the corresponding metallabis(dicarbollide), we obtained the aqueous solubility value of each complex. Hence, UV-vis spectroscopy has been a good technique for estimating the aqueous solubility, and the log S values are 3.24 for Na[**5**] and 3.15 for Na[**6**]. The *meta*-metallabis(dicarbollide) isomers, which do not aggregate, display the highest aqueous solubility, while the 8,8′-I$_2$-*o*-metallabis(dicarbollide) isomers display the lowest (see Table 3).

Besides aqueous solubility, a drug's lipophilicity is a key physicochemical parameter because it determines its solubility, its permeability through membranes, and therefore its absorption, biodistribution and clearance. Lipophilicity is expressed by the *n*-octanol/water partition coefficient (log P).[51] The as-found P values are 43.7 (log P = 1.64) for Na[**1**],[44] 45.7 (log P = 1.66) for Na[**2**], 151.0 (log P = 2.18) for Na[**3**],[44] 99.3

(log P = 2.00) for Na[**4**], 26.0 (log P = 1.41) for Na[**5**] and 35.2 (log P = 1.55) for Na[**6**].

When comparing the two isomers of the same metal, Na[**1**]/Na[**5**] and Na[**2**]/Na[**6**], the *ortho*-isomers are more lipophilic than the corresponding *meta*-isomers (approximately 1.7 and 1.3-fold for the Co and Fe complexes, respectively). While comparing the same isomer but a different metal, (Na[**1**]/Na[**2**] and Na[**5**]/Na[**6**], the iron provides a more lipophilic character than the cobalt, with the effect being higher in the *meta*-isomers. When comparing the effect of the two iodine atoms, Na[**1**]/Na[**3**] and Na[**2**]/Na[**6**], the lipophilicity increased with the presence of the two iodine atoms in both the iodinated couples (approximately 3.5 and 2.2-fold for the Co and Fe complexes, respectively). Consequently, the ligand's isomerism (*ortho*-/*meta*-) as well as the nature of the metal (Co/Fe) significantly affects the lipophilicity of the small metallabis(dicarbollide) molecule.

Lipophilicity is a major factor influencing passive transfer to or from the brain across the blood–brain barrier (BBB). Typically, for a radiotracer to be considered as a potential efficient molecular imaging probe in the living human brain with positron emission tomography (PET), its partition coefficients (log P) should range between 2.0–3.5.[52] The metallabis(dicarbollide) complexes with log P in this range are the di-iodinated Na[**3**] and Na[**4**] (Table 3).

Antimicrobial studies

Although biological studies on cancer cells have been reported for [**1**]$^-$ and [**5**]$^-$,[26] no studies of the small inorganic amphiphilic molecule $[M(C_2B_9H_{11})_2]^-$ (M = Co^{3+}, Fe^{3+}) parents as antimicrobial agents have been reported yet. Chart 2 displays the reported cobaltabis(dicarbollide) derivatives with tested anti-

Dalton Transactions

Table 3 The chemical and physicochemical parameters of the metallabis(dicarbollide) complexes studied

Parameters	[1]⁻	[2]⁻	[3]⁻	[4]⁻	[5]⁻	[6]⁻
Size (nm) = $L \times W$(max) L = length and W = width (ref. 50)	1.04 × 0.53 (ref. 38)	1.01 × 0.56 (ref. 49)	1.02 × 0.75 (ref. 27a)	1.02 × 0.75	1.01 × 0.54	1.01 × 0.54 (ref. 60)
Molecular weight of the anion	323.75	320.66	575.54	572.45	323.75	320.66
Rotamer	Cisoid	Cisoid	Transoid	Transoid	Transoid	Transoid
Intramolecular interactions	No	No	C_c–H···I	C_c–H···I	No	No
Intermolecular interactions in aqueous solution	Yes	Yes	Yes	Yes	No	No
Aggregate formation in H_2O	Yes (ref. 18 and 20c)	Yes	Yes (ref. 18)	Yes	No	No
DLS	Aggregates (ref. 44) (d = 64 nm) in the range 1 < c < 29 mM	Aggregates (d = 140 nm) in the range 1 < c < 50 mM	Aggregates (ref. 44) (d = 107 nm) in the range 1 < c < 110 mM	Aggregates (d = 83.5 nm) in the range 1 < c < 80 mM	—	—
	Aggregates (d = 1.4 nm) c > 29 mM	Aggregates (d = 108 nm) c > 50 mM	Aggregates (d = 1.1 nm) at c > 110 mM	Aggregates (d = 1.5 nm) at c > 80 mM		
Solubility in H_2O (mM)	1509 (ref. 26)	1247	210 (ref. 26b)	374	1726	1.400
log S	3.18	3.10	2.32	2.57	3.24	3.15
Lipophilicity (P)	43.7	45.7	151.0	99.3	26.0	35.2
log P	1.64	1.66	2.18	2.00	1.41	1.55
$E_{1/2}$ M$^{3+/2+}$(in V reference F_c^+/F_c)	−1.80	−0.73	−1.33	−0.36	−1.55	−0.79
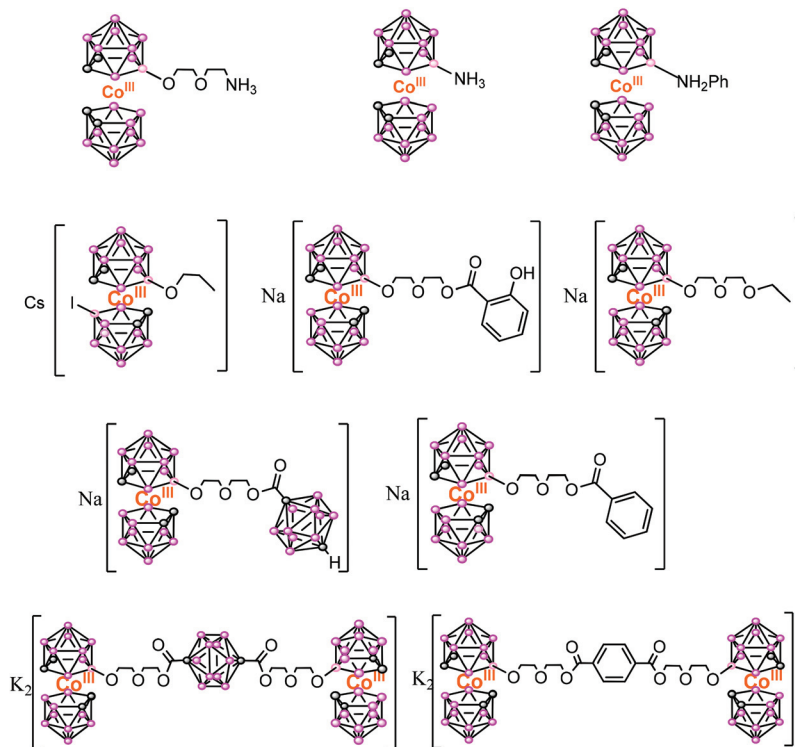
Chart 2 Reported cobaltabis(dicarbollides) with effective antimicrobial properties.[53,54]

microbial properties; the three compounds with the amino group are zwitterionic while the others are mono- and di-anionic.

Chart 1 shows the six small anionic metallabisdicarbollide molecules tested in this study to predict their potential application as antimicrobial agents. Herein, the influence of the

Table 4 Minimum inhibitory concentration (MIC) and minimum bactericidal concentration (MBC) (indicated as µM) of cobaltabis(dicarbollides) on clinical isolates that cause infection

Strain	Na[1] MIC	Na[1] MBC	Na[3] MIC	Na[3] MBC	Na[5] MIC	Na[5] MBC	Na[2] MIC	Na[2] MBC	Na[4] MIC	Na[4] MBC	Na[6] MIC	Na[6] MBC
Gram-negative bacteria												
E. coli – LF82[a]	0.653	1.307	0.050	0.050	0.082	0.082	0.649	0.649	0.250	0.400	0.165	0.329
E. coli WT – 190940	0.653	0.653	0.050	0.050	0.082	0.163	0.649	0.649	0.250	0.250	0.165	0.165
E. coli BLEE – 192348[a]	0.653	0.653	0.050	0.050	0.082	0.163	0.325	0.325	0.250	0.250	0.165	0.165
P. aeruginosa WT – 190089	0.653	0.653	0.050	0.099	0.163	0.327	0.649	0.649	0.250	0.250	0.325	0.325
P. aeruginosa IMI-R – 187182[a]	0.653	0.653	0.050	0.099	0.163	0.327	0.649	0.649	0.250	0.250	0.325	0.325
Gram-positive bacteria												
E. faecalis WT – 190093	0.041	0.082	0.012	0.012	0.041	0.041	0.041	0.041	0.025	0.025	0.021	0.021
E. faecalis WT – 194844	0.041	0.041	0.012	0.012	0.041	0.041	0.041	0.041	0.025	0.025	0.021	0.021
S. aureus WT – 180895	0.041	0.082	0.006	0.012	0.041	0.041	0.041	0.082	0.012	0.012	0.021	0.021
S. aureus MRSA – 182851[a]	0.041	0.082	0.006	0.012	0.041	0.041	0.041	0.082	0.025	0.050	0.010	0.021
Yeast												
C. albicans – 180228	0.082	0.163	0.002	>0.003	0.003	>0.010	0.041	0.082	0.012	0.025	0.005	>0.010
C. albicans – 181721	0.082	0.163	0.002	>0.003	0.003	>0.010	0.041	0.082	0.012	0.025	0.005	>0.010
C. albicans – 191026	0.082	0.163	0.002	>0.003	0.003	>0.010	0.041	0.082	0.012	0.025	0.005	>0.010

[a] Multidrug-resistant strains.

$[C_2B_9H_{11}]^{2-}$ ligand isomers (*ortho-/meta-*), the metal effect (Co^{3+}/Fe^{3+}) on the same isomer, as well as the influence of the presence of the iodine atoms on the structure–activity relationship of these as promising antimicrobial agents to tackle antibiotic-resistant bacteria was studied.

All the metallabis(dicarbollides) tested in the study had a better effect on yeast and Gram-positive bacteria than on Gram-negative bacteria. The minimum inhibitory concentration (MIC) values ranged from 0.002 to 0.082 µM for *Candida* species, from 0.006 to 0.041 µM for Gram-positives and from 0.050 to 0.653 µM for Gram-negatives (Table 4). The minimum bactericidal concentration (MBC) values indicated that these compounds had a bactericidal/fungicidal effect, since the ratio MBC/MIC was ≤2. However, while previously tested [1]⁻ derivatives with a *cisoid* conformation were highly effective against Gram-positives,[53a,54] the parent metallabis (dicarbollides) studied here had a reduced antimicrobial effect towards this group of bacteria, but increased potency against Gram-negative and *Candida* species.

Analyzing the influence of the ligands (*ortho-/meta-*). The *ortho*-isomers, Na[1] and Na[2], were the compounds with less antibacterial effect in all microbial groups, and few differences were observed between them since the MIC values were identical in all Gram-positives and the majority of Gram-negatives tested. However, the *meta*-isomers (Na[5] and Na[6]) were more effective than the *ortho*-isomers, indicating that the different isomers (*ortho-* or *meta-*) of the ligands may have a notable impact on the antimicrobial effectivity of the parent metallabis (dicarbollide) compounds. The antimicrobial effect of *meta*-metallabis(dicarbollide) with respect to the *ortho*-metallabis (dicarbollide) was particularly evident for Gram-negative and *Candida* species in the case of Na[5], and in all groups of microorganisms in the case of Na[6]. The MIC values of Na[5] were from four to eight times lower than those of Na[1] in

Gram-negative bacteria and 27 times lower in *Candida*. No differences between *ortho*-metallabis(dicarbollides) and *meta*-metallabis(dicarbollides) were observed in Gram-positive bacteria. In turn, Na[6] MIC values were from two to four times lower than Na[2] in both Gram-positive and Gram-negative bacteria and eight times lower in *Candida*.

It was experimentally demonstrated by small- and wide-angle X-ray and neutron scattering that Na[1] has a rich self-assembly behavior, being able to form monolayer vesicles and micelles in diluted aqueous solution.[20c] Besides, theoretical DFT calculations using implicit solvent found that the *cisoid* rotamer (which has a polar and an apolar region) is the most stable form of Na[1] small anionic molecules in water.[19] As stated at the beginning of this section, the DLS and NMR studies of the *meta*-metallabis(dicarbollide) indicated that these isomers do not produce aggregates and also that the crystal structure of H[5] presents a *transoid* conformation of the [5]⁻ small anionic molecule, which organizes in 2D layers leading to a lamellar arrangement of only [5]⁻ units. The *transoid* rotamers present in the *meta*-metallabis(dicarbollides), which lacks a "hydrophilic head" and a "hydrophobic tail" compared with *cisoid* rotamers present in the *ortho*-metallabis (dicarbollides), may be the key factor for *meta*-isomers being more effective than the *ortho*-isomers against Gram-negative bacteria.

Analyzing the influence of the metal ($Co^{3±}/Fe^{3±}$). The metal present in the *ortho*-metallabis(dicarbollide) structures, which provides a large difference in the $E_{1/2}$ (Table 3), had little effect because, often, the MIC values were similar between the Na[1]/Na[2] compounds, with the exception of the di-iodinated compounds. The [3]⁻ showed a notable increased antimicrobial effect in comparison with [4]⁻. Moreover, differences between cobalt and iron complexes were observed in the case of the *meta*-isomers. For all Gram-negative bacteria and *Candida* sp.

tested, Na[5] MIC values were two times lower than the MIC values of Na[6]. In contrast, Na[5] MIC values were between two and four times higher than those of Na[6] in Gram-positive bacteria. Therefore, [5]⁻ had a better antimicrobial effect against Gram-negative and *Candida albicans* whereas [6]⁻ had a better effect on Gram-positive bacteria. The fact that the difference in the $E_{1/2}$ of the couple M^{3+}/M^{2+} between the related couples Na[1]/Na[2] and Na[5]/Na[6] (−1.81/−0.73 V and −1.55/−0.79 V), respectively, does not produce a significant effect on the antimicrobial activity may suggests that the membrane translocation process does not involve any redox reactions.

In order to discern if the translocation process of the metal-labis(dicarbollide) small molecules is related to their conformation, *cisoid* for the *ortho-* and *transoid* for the *meta-*, the transoid conformation of the *ortho*-metallabis(dicarbollides) was forced with the introduction of an iodine atom in each B(8) vertex of each complex's ligand. The *transoid* rotamer is fixed in both di-iodinated [3]⁻ and [4]⁻ small molecules because of two factors: (i) the repulsion of the three lone pairs of electrons of the iodine atom of the B(8)–I bond in each ligand of the complexes and (ii) the formation of two C_c–H···I–B(8) intramolecular bonds between the C_c–H vertex from one ligand and the I–B(8) vertex from the other one. The crystal structures of Cs[3] and [4]⁻ (codes refcodes DEXPIF[42] and GANQIY[27a]), which present two-fold symmetry anions with the two iodine atoms in the trans position, support the most stable rotamer, *i.e. transoid*, in both di-iodinated metallabis(dicarbollides). Additionally, it was also proved that the [3]⁻ small anionic molecule combines the properties of purely organic surfactants and purely inorganic sheet systems, such as clays self-assembling in layers that form lyotropic lamellar phases in a concentrated regime, but that are able to bend into vesicles in a dilute regime.[55]

Analyzing the influence of the presence of the iodine atoms. Interestingly, the complexes containing two iodine groups, Na[3] and Na[4], had an improved effect against Gram-negative bacteria with respect to the corresponding parent, Na[1] and Na[2], specially the Na[3]. In Gram-negative bacteria, Na[3] MIC values were reduced thirteen times in comparison with Na[1]. This improved effect was also observed in *Candida* sp. (MIC values 52 times lower) and Gram-positive bacteria (from three to six times lower). Na[4] was also more effective, especially in Gram-negative and *Candida* species, but the increased antimicrobial effect was less clear.

In summary, the most important sodium salt of the anionic icosahedral metallabis(dicarbollide) complexes was the di-iodinated Na[3] because this compound showed an increased antimicrobial effect against all the strains tested in comparison with the parent Na[1]. Other compounds with similar antimicrobial power were Na[6] for Gram-positive bacteria, and Na[5] for *Candida* sp. Moreover, we could observe that Gram-negative bacteria and *Candida albicans* have often a similar pattern of response against the different variations of the compounds, which is different from that of Gram-positive bacteria. Probably this is due to the difference in structure and composition of their cell walls. We hypothesize that the outer membrane of Gram-negative bacteria constitutes an impermeable barrier for the majority of these compounds, and that variants such as Na[3] and Na[5], both *transoid* conformers, represent structures with particular physical–chemical properties that make these compounds more permeable for crossing this barrier.

To shed light upon this hypothesis, we performed two experiments schematically displayed at the left of Scheme 2.
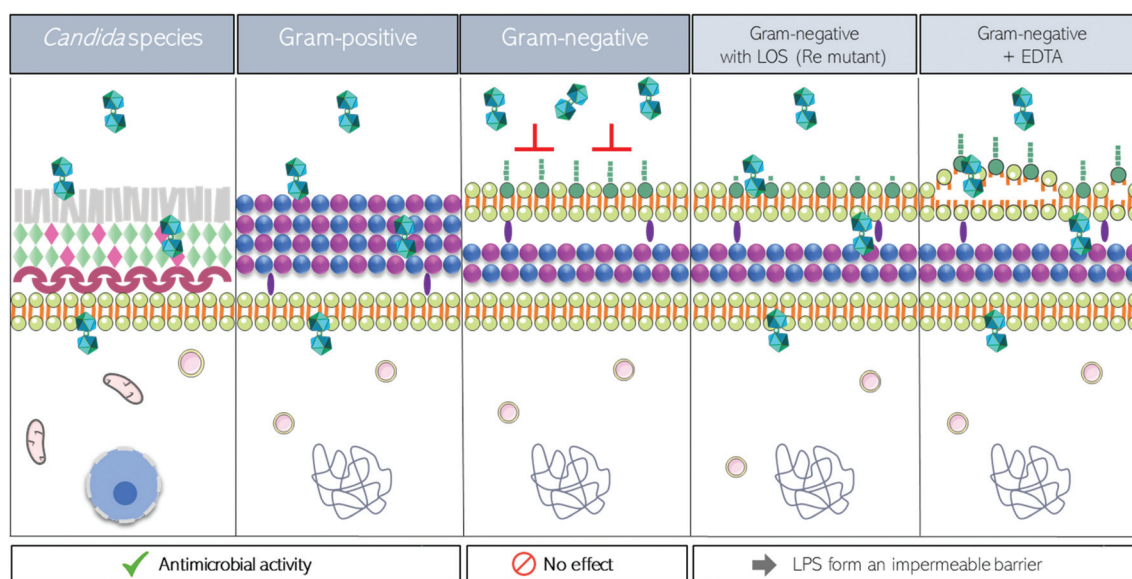
Scheme 2 Graphical representation of the transport of small anionic metallabis(dicarbollide) molecules through microbiological membranes (*Candida* sp., Gram-positive, Gram-negative, Gram-negative with LOS (Re mutant) and Gram-negative plus EDTA).

First, we studied the antimicrobial effect of Na[1] on a Gram-negative bacterial model with a mutated lipopolysaccharide (LPS), in particular the *Salmonella enterica* serotype minnesota Re 595 (Re mutant). LPS is the major component of the outer leaflet of the outer membrane of Gram-negative bacteria, which constitutes an essential structure for cell viability and prevents charged macromolecules and hydrophobic molecules entering the cell.[56] LPS are amphiphilic molecules consisting of a glycolipid portion named lipid A, which is embedded in the lipid bilayer of the outer membrane, and a saccharide portion covalently linked to the lipid A that is external. In turn, the saccharide portion consists of two main parts: (i) the core oligosaccharide, which is linked to the lipid A and is formed by sugars that are conserved between species, the first residue being the acidic sugar termed Kdo (3-deoxy-α-D-manno-oct-2-ulopyranosonic acid); and (ii) the more external polysaccharide chain named the O-chain, whose composition is variable within species. Mutants lacking the O-chain have a rough colony aspect in comparison with wild type strains that are smooth. Re mutants lack not only the O-antigen but also part of the core polysaccharide. They are formed by the lipid A and the Kdo, representing the deep-rough chemotype. Moreover, adjacent anionic LPS molecules are linked to divalent cations, mainly Mg^{2+} and Ca^{2+}, forming a compact surface and making the outer membrane more rigid than normal lipid bilayers.[57] We confirmed that these structures are essential for antimicrobial resistance in Gram-negative bacteria since the Na[1] MIC values of the Re 595 mutant decreased to 0.041 μM, and the MBC to 0.082 μM, thus having a sensibility identical to the tested Gram-positive bacteria, while the MIC was 0.65 μM for all the Gram-negative bacteria (Fig. 10).

Second, we performed an experiment combining Na[1] with ethylenediaminetetraacetic acid (EDTA). EDTA is a chelating agent that forms a complex with divalent calcium and magnesium cations present in the outer membrane of Gram-negative bacteria, destabilizing it and thus permeabilizing it.[57] A checkerboard dilution method (see Experimental section) was

carried out to unambiguously identify whether there is a synergy or additive effect between Na[1] and EDTA or not. For this analysis, *Escherichia coli* BLEE strain 192348, *Salmonella minnesota* strain Re 595 (Re mutant) and *Staphylococcus aureus* MRSA strain 18285 were used as models of a Gram-negative bacterium with intact LPS, a Gram-negative bacterium with mutated LPS, and a Gram-positive bacterium (all lacking an outer membrane), respectively. The MIC of EDTA for these strains was 7 μM, 0.22 μM, and 0.22 μM, respectively.

Fractional inhibitory concentration index (FICI) values (Table 5) and isobolograms (Fig. 11) clearly showed that there is a synergistic or additive effect between Na[1] and EDTA for the Gram-negative *E. coli* BLEE strain 192348 since, when these two compounds are used in combination, both MIC values are decreased. In contrast, no effect was observed for the Gram-positive *Staphylococcus aureus* MRSA strain 18285, and the same occurred for the LPS-mutated *Salmonella minnesota* strain Re 595 (Re mutant). These results strongly suggest that the LPS of the Gram-negative outer membrane plays a crucial role in the natural resistance of Gram-negative bacteria towards Na[1] and other related compounds.

We have demonstrated that the outer membrane of Gram-negative bacteria constitutes an impermeable barrier for the majority of these compounds, and that variants such as the derivatives [3]⁻ and [5]⁻, both *transoid* conformers, in contrast to [1]⁻, which is *cisoid*, represent structures with particular physical–chemical properties that make the compounds more permeable for crossing this barrier. While the data are still too sparse for any specific structure–activity relationship evaluation, we believe this study can serve as an important roadmap for additional studies to gain a more in-depth understanding of the mechanism of action of these metallabis(dicarbollides).

The Na[1] cytotoxicity was tested on U87 and T98G glioblastoma cells, A375 melanoma cells and non-tumoral V79 fibroblasts,[16] and the cytotoxicity of Na[3] was tested against U87
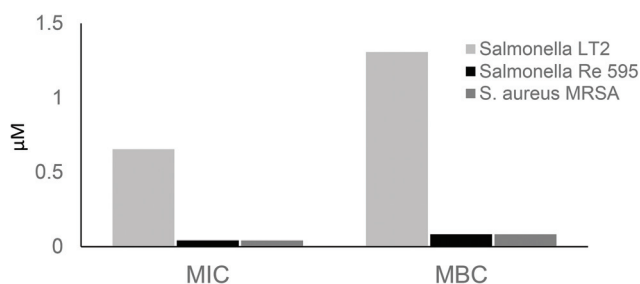
Fig. 10 Na[1] minimum inhibitory concentration (MIC) and minimum bactericidal concentration (MBC) towards *Salmonella enterica* subsp. enterica serovar Typhimurium str. LT2, *Salmonella minnesota* strain Re 595 (Re mutant) and *Staphylococcus aureus* MRSA strain 182851. The Re mutant, that contains only the lipid A and 2-keto-3-deoxyoctonate moiety of the lipopolysaccharide, shows a reduced MIC and MBC in comparison with *Salmonella* LT2 and other Gram-negatives tested and resemble *Staphylococcus aureus* MRSA strain 18285 and the other Gram-positives tested.

Table 5 FICI values of Na[1] and EDTA combination against *Esherichia coli* BLEE strain 192348, *Salmonella minnesota* strain Re 595 (Re mutant) and *Staphylococcus aureus* MRSA strain 18285

Strain	MIC Na [1] (μM)	MIC EDTA (μM)	FICI	Interpretation
E. coli BLEE strain 192348	0.653	0.000	—	—
	0.327	0.109	0.516	Additivity
	0.163	0.219	0.281	Synergy
	0.041	0.438	0.125	Synergy
	0.041	0.876	0.188	Synergy
	0.041	1.752	0.313	Synergy
	0.041	3.504	0.563	Additivity
	0.000	7.008	—	—
Salmonella strain Re 595 and *S. aureus* MRSA strain 18285	0.041	0.000	—	—
	0.041	0.007	1.031	Indifference
	0.041	0.014	1.063	Indifference
	0.041	0.027	1.125	Indifference
	0.041	0.055	1.25	Indifference
	0.041	0.109	1.5	Indifference
	0.000	0.219	—	—
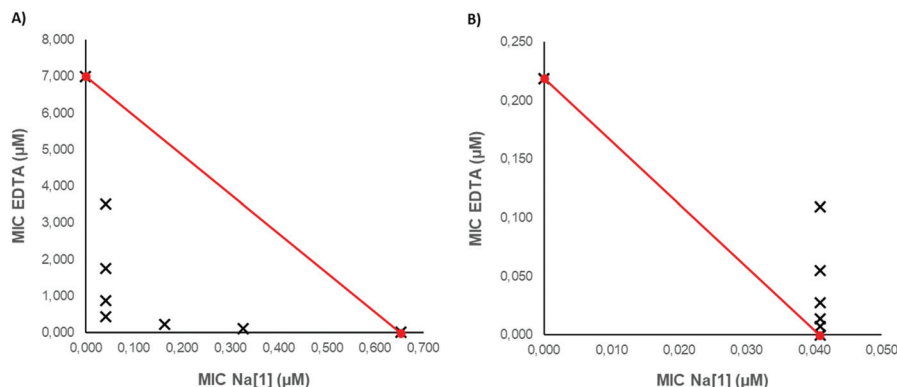
Fig. 11 Isobologram analyses. MIC concentrations of Na[**1**] are plotted on the *x*-axis and MIC values of EDTA on the *y*-axis. (A) Isobologram for *Escherichia coli* BLEE strain 192348 and (B) *Salmonella minnesota* strain Re 595 (Re mutant) and *Staphylococcus aureus* MRSA strain 18285. Crosses indicate the MIC values obtained in the checkerboard dilution method. In red, the "indifference line" where crosses below indicate a synergistic or additive effect, whereas crosses above indicate no interaction or indifference.

and T98G glioblastoma cells.[44] The IC_{50} (compound concentration causing 50% inhibition of cell growth) is a parameter used to evaluate the cytotoxicity of a given compound. The IC_{50} values at 24 h of incubation time with Na[**1**] and/or Na[**3**] ranged from 59 μM to 195 μM, displaying no relevant cytotoxic activity, whereas the MIC values for the microorganisms tested here ranged from 0.002 μM to 0.653 μM. The ratio IC_{50}/MIC has been used to calculate the selectivity index (SI) for antimicrobial compounds,[58] and it is considered that an SI ≥ 10 is acceptable for a selective bioactive sample.[59] The ideal drug should be biologically active at a very low concentration and toxic only at a very high concentration. Taking as a reference the lowest IC_{50} and the highest MIC for each compound (the worst situation), the SI for both compounds is very high: Na[**1**] = 165 (IC_{50} for V79 cells: 102 μM/MIC for Gram-negative: 0.653 μM), and Na[**3**] = 1180 (IC_{50} for T98G cells: 59 μM/MIC for Gram-negative: 0.05 μM). The high value of the selectivity indices for Na[**1**] and Na[**3**] indicate that these compounds may be useful in managing bacterial and fungal infections.

The fact that these small anionic molecules can cross the mammalian membrane and have antimicrobial properties but low toxicity for mammalian cells represents a promising tool to treat infectious intracellular bacteria. Future experiments determining the effectivity of these compounds during *in vitro* infection will shed light on this question.

Conclusions

We have reported here the synthesis of several sodium salts of the small anionic metallabis(dicarbollide) molecules ([$M(C_2B_9H_{11-n}X_n)_2$]$^-$, M = Co^{3+}, Fe^{3+}, n = 1, X = H or I): Na[**4**], Na[**5**] and Na[**6**] and their full characterization by FTIR, ^{1}H, ^{1}H{^{11}B}, ^{11}B, ^{11}B{^{1}H} NMR, UV-vis, and MALDI-TOF-MS spectroscopy. The solubility and lipophilicity of the sodium salts of the parent anionic small metallabis(dicarbollide) molecules ([**1**]$^-$, [**2**]$^-$, [**3**]$^-$, [**4**]$^-$, [**5**]$^-$ and [**6**]$^-$), which are very important

for understanding their biological behavior, are reported. The *meta*-isomers (Na[**5**] and Na[**6**]) display the highest aqueous solubility while the 8,8′-I$_2$-*o*-metallabis(dicarbollide) isomers (Na[**3**] and Na[**4**]) display the lowest. Aggregate formation of the four *ortho* metallabis(dicarbollides) (Na[**1**], Na[**2**], Na[**3**] and Na[**4**]) in aqueous solution was studied using DLS, TEM and CryoTEM while no aggregates were observed by DLS and ^{1}H{^{11}B}-NMR for the *meta*-isomers of the metallabis(dicarbollides). The redox behavior of the sodium salt of the six complexes, corresponding to the redox couples M$^{3+/2+}$, has been studied by mean of CV, observing reversible processes in all cases. In general, *ortho*- and *meta*-Co^{3+} small molecules are more reducing than the corresponding Fe^{3+} ones, but their iodine derivatives are less reducing in both cases. The *ortho*-isomer, [**1**]$^-$, is more reducing than the *meta*-isomer[**5**]$^-$; however the opposite effect is observed in the case of the Fe^{3+} complexes.

The X-ray structures of the protonated salt of the [**5**]$^-$, [($H_3O)(H_2O)_5$][2,2′-Co(1,7-$C_2B_9H_{11}$)$_2$], and the cesium salt of the [**3**]$^-$, [Cs(MeCN)][8,8′-I$_2$-Fe(1,2 $C_2B_9H_{10}$)$_2$], are reported. Both crystal structures display *transoid* conformation of the [$M(C_2B_9H_{11})_2$]$^-$ cluster. The supramolecular structure of the protonated salt of [**5**]$^-$ presents 2D layers leading to a lamellar arrangement of the small anion molecules, while the cationic part is formed of polymeric water rings made of six- and four-membered rings of water molecules connected *via* OH···H hydrogen bonds. The water layers with weak B–H···O contacts help to connect the cationic and anionic layers.

We have demonstrated an antimicrobial effect of these small metallabis(dicarbollide) anionic molecules against *Candida* species, and against Gram-positive and Gram-negative bacteria, including multiresistant strains. The selectivity index for antimicrobial activity of the compounds Na[**1**] and Na[**3**] is very high (165 and 1180, respectively) indicating these compounds may be useful in managing bacterial and fungal infections. This article reveals that small anionic metallabis(dicarbollide) molecules with activities down to the nanomolar

range against methicillin resistant *S. aureus* (MRSA) and a high selectivity index are promising antimicrobial agents to tackle antibiotic-resistant bacteria. It remains to be determined whether the compounds' concentrations needed to cause an antimicrobial effect *in vitro* would be applicable, and effective, *in vivo*. Moreover, we have demonstrated that the outer membrane of Gram-negative bacteria constitutes an impermeable barrier for the majority of these compounds. Nonetheless, changes in the structure of the parent molecule Na[**1**], such as the *meta*-isomers or the addition of two iodine groups, had an improved effect against Gram-negative bacteria, possibly due to changes in their physicochemical properties in aqueous media that make the *meta*-isomers and the di-iodinated *ortho*-small molecules more permeable for crossing this barrier. To emphasize, the most active metallabis(dicarbollide) small molecules are both *transoid* conformers, in contrast to [**1**]⁻, which is *cisoid*. Since there is an urgent need for antibiotic discovery and development, this study represents a relevant advance in the field.

Experimental section

Materials

The NaCl was purchased from Sigma–Aldrich, whereas the cationic exchanging resin used (Amberlite IR120, H form) was purchased from Acros Organics and the hydrochloric acid (37%) was purchased from Carlo Erba Reagents. Solvents used were from Carlo Erba SDS and purified by distillation from sodium and benzophenone under a nitrogen atmosphere before use. Na[3,3′-Co(1,2-C$_2$B$_9$H$_{11}$)$_2$]·2.5H$_2$O abbreviated as Na[**1**],[18] Na[3,3′-Co(8-I-1,2-C$_2$B$_9$H$_{10}$)$_2$]·2.5H$_2$O abbreviated as Na[**3**],[18] and Na[**2**]·2.5H$_2$O abbreviated as Na[**2**][37] were synthesized as reported in the literature. [NMe$_4$][2,2′-Co(1,7-C$_2$B$_9$H$_{11}$)$_2$] abbreviated as [NMe$_4$][**5**][35] and [NMe$_4$][2,2′-Fe(1,7-C$_2$B$_9$H$_{11}$)$_2$] abbreviated as [NMe$_4$][**6**] were synthesised according to the literature with some modifications.[60]

Instrumentation and measurements

FTIR spectra were run using a Shimadzu FTIR-8300 spectrophotometer. The ^{1}H, ^{1}H{^{11}B} NMR (400.13 MHz) and ^{11}B and ^{11}B{^{1}H} NMR (128.37 MHz) spectra were recorded on a Bruker ARX 400 instrument equipped with the appropriate decoupling accessories. All NMR spectra were performed in the indicated deuterated water at 22 °C. The ^{11}B and ^{11}B{^{1}H} NMR chemical shift values were referenced to external BF$_3$·OEt$_2$, while the ^{1}H, ^{1}H{^{11}B} NMR chemical shift values were referenced to SiMe$_4$. Chemical shifts are reported in units of parts per million downfield from the reference. The mass spectra were recorded in the negative ion mode using a Bruker Biflex MALDI-TOF-MS [N$_2$ laser; λ_{exc} 337 nm (0.5 ns pulses); voltage ion source 20.00 kV (Uis1) and 17.50 kV (Uis2)].

Cyclic voltammogram responses were recorded at a glassy carbon electrode in MeCN of 0.1 M [NnBu$_4$][PF$_6$] as the supporting electrolyte, with a metallabis(dicarbollide) concentration of 5 mM at a scan rate of 50 mV s^{-1} on a Autolab

PGSTAT204 potentiostat, controlled by Nova 2.1.4 software by Metrohm Autolab. The electrochemical cell contained Ag/AgCl/[NBu$_4$]Cl as the reference electrode, a glassy carbon as the working electrode and Pt wire as the counter one. All experiments were performed at room temperature. The solutions were deaerated with analytical grade nitrogen at the start of each experiment to prevent oxygen interference. All the potential values were referred to the F$_c^+$/F$_c$ couple ($E_{1/2}$ (F$_c^+$/F$_c$) = 0.64 V *vs.* the standard hydrogen electrode (SHE)). UV-vis spectra were recorded on a Jasco V-780 spectrophotometer, using 1 cm cuvettes with 0.08 mM of metallabis(dicarbollides) in water. The hydrodynamic diameter of the samples dispersed in water were studied by dynamic light scattering (DLS) in a Zetasizer Nano ZS (Malvern Instruments Ltd) equipped with a He–Ne 633 nm laser using 1 mL of the sample's dispersion in a disposable glass cuvette. For each compound a couple of samples were run, and the measurements were done in triplicate at ambient temperature with multiple sub-runs. The aqueous sample solutions were previously filtered using a syringe filter (PTFE, 0.2 μm pore diameter). Thermogravimetric analyses/differential scanning calorimetry (TGA/DSC) were performed on a Netzsch STA 449 thermal analyzer at a heating rate of 10 °C min^{-1} under an Ar atmosphere.

Synthesis and characterization of Cs[3,3′-Fe(8-I-1,2-C$_2$B$_9$H$_{10}$)$_2$], Cs[4]

Cs[**4**] was synthesized from Cs[**2**]. 50 mg (0.11 mmol) of Cs[**2**] was mixed with 49.2 mg (0.22 mmol) of *N*-iodosuccinimide and dissolved in 20 mL of ethanol. Subsequently, 0.2 mL (2.27 mmol) of CF$_3$SO$_4$H was added drop by drop, then the reaction flask was closed, and lead react at room temperature for 3 hours. Once the reaction was finished, the solvent was removed under reduced pressure and the product was extracted in THF and a saturated solution of NaCl in 0.1 M HCl solution three times; the organic layer was then dried. Finally, the residue was redissolved in water and a saturated solution of CsCl was added, promoting the precipitation of 146 mg (94% yield) of a dark green product Cs[**4**]. MALDI-TOF-MS: Theor. 572.45 *m/z*. Found 573.17 *m/z*. ^{1}H{^{11}B} NMR (400 MHz, CD$_3$COCD$_3$) δ: 123.10, 58.72 (s, B–H), 43.68 (4H, s, C$_{cluster}$–H), 6.82, 1.32, −0.96 and −20.77 (s, B–H). ^{11}B NMR (128.37 MHz, CD$_3$COCD$_3$) δ: 121.8 (2B, B(6,6′), B–H), 26.3 (4B, B(5,5′,11,11′), B–H), 8.3 (4B, (B9,9′,12,12′), B–H), −46.8 (2B, B(10,10′), B–H), −334.9 (4B, B(4,4′,7,7′), B–H) and −568.3 (2B, B(8,8′), B–I).

Synthesis and characterization of Na[3,3′-Fe(8-I-1,2-C$_2$B$_9$H$_{10}$)$_2$]·2.5H$_2$O, Na[4]

Na[**4**] was obtained by means of the cationic exchange resin from Cs[3,3′-Fe(8-I-1,2-C$_2$B$_9$H$_{10}$)$_2$]. Approximately 2/3 of the volume of the column (30 cm) was filled with the strongly acidic cationic exchange resin (Amberlite IR120, H form). Before starting, the cationic resin was maintained for 24 h in HCl 3 M to hydrate it. Then, 150 mL of a solution of HCl 3 M was slowly passed through the column to load it with H$^+$. To remove the excess of HCl, distilled water was flowed quickly

down the column until a neutral pH was reached. When the desired cation was sodium, a solution of NaCl 3 M was passed through the column slowly to exchange H^+ by Na^+ until a neutral pH was reached. Distilled water was used to rinse the excess of NaCl through the column. To know if NaCl had been removed, 3 drops of a solution of $AgNO_3$ 100 mM were added to a small fraction of the solution coming out of the column until a clear solution was observed. Then, 30 mL of acetonitrile/water (50 : 50) mixture was flowed through the column to set the column's liquid composition. Approximately 200 mg of Cs[**4**] was dissolved in a minimum volume of acetonitrile/water (50 : 50) and flowed repeatedly (4 times) through the cationic resin. Before collecting the solution containing the ferrabis(dicarbollide), 50 mL of fresh acetonitrile/water (50 : 50) was added to the column. 50 mL were collected in a flask, the solvent was evaporated and the compound was dried under vacuum. FTIR $\nu(cm^{-1})$ = 3586, 3492 (O–Na), 3031, 3017 ($C_{cluster}$–H), 2578, 2552, 2528 (B–H), 1688, 1611 (H_2O). $^1H\{^{11}B\}$ NMR (400 MHz, CD_3COCD_3) δ: 117.79, 56.31 (s, B–H), 42.16 (4H, s, C_c–H), 1.05, −0.77, −6.07 and −20.20 (s, B–H). ^{11}B NMR (128.37 MHz, CD_3COCD_3) δ: 114.7 (2B, B(6,6′), B–H), 23.8 (4B, B(5,5′,11,11′), B–H), 6.1 (4B, (B9,9′,12,12′), B–H), −47.1 (2B, B(10,10′), B–H), −322.34 (4B, B(4,4′,7,7′), B–H) and −548.91 (2B, B(8,8′), B–I).[61] MALDI-TOF-MS: Theor. 572.45 m/z. Found 573.14 (M, 100%) m/z, where M is the molecular weight of the anion [**4**]⁻. Solubility of Na[**4**] = 374 mM. Anal. Calcd for $C_4H_{20}B_{18}NaFeI_4\cdot2.5H_2O$: C: 7.49, H: 3.98. Found: C: 7.55, H: 3.93. TGA/DSC: two exothermic weight losses of 1.62 and 2.38% until 160 °C, and 18.82 at 570 °C; the residual mass is 77.98% at 800 °C.

Synthesis and characterization of Na[2,2′-Co(1,7-$C_2B_9H_{11}$)$_2$]·2.5H_2O, Na[5]

Na[**5**] was obtained by the cation exchange procedure using [NMe₄][**5**] as the starting material.[35b] The yellowish ion exchange resin was maintained for 24 h in HCl solution (3 M), and then used to fill approximately 2/3 of a column. A solution of HCl (3 M) was passed through this column until a transparent solution was obtained. The excess of HCL was removed by rinsing the resin using distilled water until a neutral pH was reached. A solution of NaCl (3 M) was passed slowly through the column to change the H^+ to Na^+. Distilled water was used in order to remove the excess of NaCl. Subsequently, an acetonitrile/water (50/50) mixture was flowed through the column, and the minimum amount of the same solution was used to dissolve the Cs[**5**]. This orange solution was passed several times through the column, and then collected, evaporated and dried in vacuum. FTIR $\nu(cm^{-1})$ = 3595, 3374(O–Na), 3039 (C_c–H), 2539 (B–H), 1610 (H_2O). $^1H\{^{11}B\}$ NMR (400 MHz, D_2O) δ: 3.55 (s, B–H), 2.97 (4H, s, C_c–H), 2.88, 1.64 (s, B–H). ^1H NMR (400 MHz, D_2O) δ = 2.96 (4H, s, $C_{cluster}$–H). $^1H\{^{11}B\}$ NMR (400 MHz, CD_3COCD_3) δ: 3.54, 3.02 (s, B–H). 2.97 (4H, s, $C_{cluster}$–H), 1.85, 1.72 (s, B–H). ^1H NMR (400 MHz, CD_3COCD_3) δ: 2.97 (4H, s, $C_{cluster}$–H). ^{11}B NMR (128.37 MHz, CD_3COCD_3) δ: 1.2 (2B, d, ^1J(B,H) 141, B–H), −2.3 (4B, d, ^1J(B,H) 152, B–H), −9.2 (2B, d, ^1J(B–H) 160, B–H), −12.1 (6B, d, ^1J(B,H) 150, B–H),

−17.7 (4B, d, ^1J(B–H) 159, B–H). ^{11}B NMR (128.37 MHz, CD_3COCD_3) δ: 1.2 (2B, d, ^1J(B,H) 141, B–H), −2.3 (4B, d, ^1J(B, H) 152, B–H), −9.2 (2B, d, ^1J(B–H) 160, B–H), −12.1 (6B, d, ^1J(B,H) 150, B–H), −17.7 (4B, d, ^1J(B–H) 159, B–H). MALDI-TOF-MS: Theor. 323.75 m/z. Found 324.38 (M, 100%) m/z, where M is the molecular weight of the anion [**5**]⁻. Solubility of Na[**5**] = 1726 mM.

Synthesis and characterization of Na[2,2′-Fe(1,7-$C_2B_9H_{11}$)$_2$], Na[6]

The same procedure and amounts as those for Na[**5**] were used, but starting from [NMe₄][**6**] to obtain the Na[**6**]. $^1H\{^{11}B\}$ NMR (400 MHz, CD_3COCD_3) δ: 66.80 (s, B–H), 53.76 (4H, s, $C_{cluster}$–H), 6.74, 3.86, 1.19, 0.80, and −0.11 (s, B–H). ^{11}B NMR (128.37 MHz, CD_3COCD_3) δ: 33.77 (2B, B–H), 26.61(2B, B–H), 10.15 (2B, B–H), −4.49 (2B, B–H), −21.44 (2B, B–H), −35.32 (2B, B–H), −328.78(4B, B(6,6′,11,11′), B–H) and −408.45 (2B, B(9,9′), B–H). MALDI-TOF-MS: Theor. 320.66 m/z. Found 321.38 m/z. Solubility of Na[**6**] = 1400 mM.

Single X-ray diffraction studies

X-ray structure determinations of H[5], [(H₃O)(H₂O)₅][2,2′-Co(1,7-$C_2B_9H_{11}$)$_2$]. A pale orange-yellow block-like specimen of $C_4H_{35}B_{18}CoO_6$, approximate dimensions 0.150 mm × 0.200 mm × 0.200 mm, was used for the X-ray crystallographic analysis. The X-ray intensity data were measured on a Bruker D8 QUEST ECO system equipped with a doubly curved silicon crystal Bruker Triumph monochromator and a MoKα sealed X-ray tube (λ = 0.71073 Å). A total of 1749 frames were collected. The total exposure time was 1.79 hours. The frames were integrated with the Bruker SAINT software package using a narrow-frame algorithm. The integration of the data using a monoclinic unit cell yielded a total of 26 669 reflections to a maximum θ angle of 27.50° (0.77 Å resolution), of which 1284 were independent (average redundancy 20.770, completeness = 99.8%, R_{int} = 4.52%, R_{sig} = 1.45%), and 1228 (95.64%) were greater than $2\sigma(F^2)$. The final cell constants of a = 8.0526(3) Å, b = 11.2324(5) Å, c = 12.1312(6) Å, β = 103.702(2)°, volume = 1066.04(8) Å³, are based upon the refinement of the XYZ-centroids of 88 reflections above 20$\sigma(I)$ with 6.537° < 2θ < 45.04°. Data were corrected for absorption effects using the multi-scan method (SADABS). The ratio of minimum to maximum apparent transmission was 0.938. The calculated minimum and maximum transmission coefficients (based on crystal size) are 0.8530 and 0.8860.

The structure was solved and refined using the Bruker SHELXTL software package,[62] using the space group $C12/m1$, with Z = 2 for the formula unit, $C_4H_{35}B_{18}CoO_6$. The final anisotropic full-matrix least-squares refinement on F^2 with 80 variables converged at $R1$ = 2.73% for the observed data, and w$R2$ = 7.52% for all data. The goodness-of-fit was 1.202. The largest peak in the final difference electron density synthesis was 0.354 e⁻ Å⁻³ and the largest hole was −0.291 e⁻ Å⁻³ with an RMS deviation of 0.059 e⁻ Å⁻³. On the basis of the final model, the calculated density was 1.345 g cm⁻³ and F(000), 446 e⁻.

X-ray structure determinations of Cs[4], [Cs(MeCN)][4]

The measured crystals were prepared under inert conditions immersed in perfluoropolyether as a protecting oil for the manipulation. Suitable crystals were mounted on MiTeGen MicroMounts and used for data collection. Crystallographic data for Cs[4] were collected at 100 K with a XALOC beamline at the ALBA Synchrotron (λ = 0.82652 Å). Crystallographic data for compound Cs[4] were collected with a Bruker D8 Venture diffractometer. Data were processed with the APEX3 program,[63] and corrected for absorption using SADABS.[64] The structure was solved by direct methods and subsequently refined by correction of F^2 against all reflections[62] and Olex2 as the graphical interface.[65] All non-hydrogen atoms were refined with anisotropic thermal parameters by full-matrix least-squares calculations on F^2. All hydrogen atoms were located in difference Fourier maps and included as fixed contributions riding on attached atoms with isotropic thermal displacement parameters 1.2 or 1.5 (-methyl) times those of the respective atom.

A summary of the crystal data is reported in the ESI (Table S1†). CCDC 2149703 for $[(H_3O)(H_2O)_5][2,2'-Co(1,7-C_2B_9H_{11})_2]$, H[5]) and 2149633 (for [Cs(MeCN)][4] present the crystallographic data of these new crystal structures.†

Partition coefficient (P) measurement. Different amounts of Na[2], Na[4], Na[5], and Na[6] were added to a 10 ml vial containing 3 ml of *n*-octanol. Once the amount of metallacarborane was dissolved, 3 ml of deionized water was added. The different vials were horizontally and vigorously shaken at room temperature for 2 h to ensure the compound's transfer between the two phases and then the vials were left for 1 h before centrifuging for 10 minutes at 6000 rpm. Finally, the organic and the aqueous phases were transferred to a UV cell and the UV absorption was measured in a Jasco UV-Vis spectrophotometer (n = 3 per each metallabis(dicarbollide), at a maximum absorbance of 278 and 272 nm for Na[2], in *n*-octanol and water, respectively; at a maximum absorbance of 283 nm for Na[5], in water; at a maximum absorbance of 280.5 and 278.5 nm for Na[6], in *n*-octanol and water, respectively; and 288.5 and 285 nm for Na[4], again in *n*-octanol and water, respectively (see ESI†). The interpolation of the obtained values in the previously prepared quantification curves allowed knowing the concentration of the corresponding metallabis (dicarbollide) in each phase. Due to the partial solubility of *n*-octanol in water, 0.032 g per 100 g at 25 °C, and of water in *n*-octanol, 3.8 g per 100 g, the calibration curves were prepared with water-saturated *n*-octanol and *n*-octanol-saturated water, in order to avoid any possible medium interference.

Microorganisms and growth media

Clinical bacterial (N = 9) and yeast (N = 3) isolates previously tested for susceptibility to other metallacarborane compounds were used here.[54] As Gram-negative bacteria, three strains of *Escherichia coli* and two of *Pseudomonas aeruginosa* were tested, including strains that are susceptible to commonly used antimicrobials (*E. coli* 190940 and *P. aeruginosa* 190089) or are

multidrug resistant (*E. coli* BLEE 192348, *E. coli* LF82 and *P. aeruginosa* IMI 187182). As Gram-positive bacteria, we tested two *Enterococcus faecalis* strains (*E. faecalis* 190093 and *E. faecalis* 194844), and two of *Staphylococcus aureus* (*S. aureus* MRSA 182851, which is multidrug-resistant, and *S. aureus* 180895). Yeast strains belonged to the species *Candida albicans* (*C. albicans* 180228, *C. albicans* 181721 and *C. albicans* 191026). *Salmonella enterica* subsp. enterica serovar Typhimurium str. LT2 and *Salmonella minnesota* strain Re 595 (Re mutant) ATCC® 49284 ™, were used as controls to test the effect of the outer membrane lipopolysaccharide on bacterial susceptibility to the compounds.

Luria–Bertani (LB) broth was used for growing the *E. coli* and *Salmonella* species, brain heart infusion (BHI) for *P. aeruginosa*, *E. faecalis*, and *S. aureus*, and brain heart agar (BHA) for *C. albicans*.

Determination of minimum inhibitory concentrations (MIC) and minimum bactericidal concentrations (MBC)

The MIC was determined by broth microdilution following standardized guidelines,[66] and the MBC by counting viable cells at MIC, MIC × 2 and MIC × 4 concentrations following the CLSI standard protocols.[67]

Bacteria were grown in LB (*E. coli*) or BHI (*P. aeruginosa, E. faecalis*, and *S. aureus*) for 16–18 h at 37 °C without shaking. The optical density (OD) of overnight bacterial cultures was measured at 620 nm, and bacterial suspensions were prepared at a final concentration of 1×10^6 CFU mL^{-1} in cation-adjusted Mueller–Hinton (MH) broth using this relation: OD620 nm of $0.1 \approx 1.6 \times 10^8$ CFU mL^{-1}. *Candida* inoculums were prepared by resuspending five individual colonies in at least 3 mL of sterile water. The optical density was measured at 530 nm, and suspensions were prepared in sterile water at a final concentration of $(1–5) \times 10^5$ CFU mL^{-1}.

The compound stock solutions were prepared at 1024 mg L^{-1} with sterile Milli-Q water and maintained at −20 or 4 °C for a maximum of 1 month. For the bacterial tests, serial dilutions of the compounds were prepared in cation-adjusted Mueller–Hinton broth in a polystyrene 96-well plate. The concentrations tested were 512, 256, 128, 64, 32, 16, 8, 4, 2, 1, 0.5, 0.25, 0.125, and 0 mg L^{-1}. Bacteria were inoculated at a final concentration of 5×10^5 CFU mL^{-1} in a final volume of 100 µL. Microplates were incubated for 18 h at 37 °C under aerobic conditions.

The medium used to test *Candida* was RPMI with 2% glucose and ʟ-glutamine, and the concentrations of the metallabis(dicarbollide) compounds tested were 128, 64, 32, 16, 8, 4, 2, 1, 0.5, 0.25, 0.125, and 0 mg L^{-1}. The test was done in a final volume of 200 µL with $(1–5) \times 10^5$ CFU mL^{-1} per well.

Microplates were incubated for 24 h at 37 °C under aerobic conditions. All tests were done in triplicate.

The MIC was determined as the lowest concentration of the compound (indicated in µM) needed to inhibit the growth of the microorganism, which was observed by the absence of visible growth in the well. The MBC was determined by plating 20 µL of the suspension corresponding to the MIC and the two

subsequent concentrations tested (MIC × 2 and MIC × 4) onto LB agar plates that did not contain the compound. The MBC was determined as the lowest concentration of compound that reduced the viability of the initial bacterial inoculum at ≥99.9%.

Checkerboard dilution and isobologram

Na[1] was tested in combination with EDTA, an outer membrane permeabilizer, in order to evaluate the impact of the outer membrane on Na[1] ineffectiveness in Gram-negative bacteria. To do so, a checkerboard dilution method was carried out.[68] Briefly, Na[1] was serially diluted in MHB along the abscissa of 96-well plates, while EDTA was diluted along the ordinate. The initial concentration for both compounds was the MIC for each bacterium, and it was further two-fold diluted. Each well was inoculated with a bacterial inoculum of 1×10^6 cfu ml^{-1}, with a final concentration of 5×10^5 cfu ml^{-1} in a final volume of 200 µl. Plates were incubated aerobically at 37 °C for 18 ± 2 h. All the experiments were realized in triplicate.

To check the combinatorial effect of the compounds, the fractional inhibitory concentration index (FICI) was calculated as follows: FICI = (MIC EDTA in combination/MIC EDTA) + (MIC Na[1] in combination/MIC Na[1]). The combination is considered synergistic when FIC ≤ 0.5, additive when 0.5 ≤ FICI ≤ 1, indifferent when 1 ≤ FICI ≤ 4, and antagonistic when FICI > 4.[68]

An isobologram represents the results of the checkerboard assay and the FICI values. The *x*-axis represents Na[1] and the *y*-axis EDTA. The line connecting the MIC value of both compounds is the line of indifference (no interaction). Below the line of indifference are additive (1 > FICI > 0.5) and synergistic (FICI ≤ 0.5) interactions. Above the line are indifferent (1 < FICI < 4) and antagonistic (FICI ≥ 4) interactions.[69]

Author contributions

Clara Viñas: conceived and supervised the study. Margarita Martinez-Medina: designed and supervised the biological studies. Ines Bennour, Ana B. Buades: synthesis and characterization of metallabis(dicarbollides). M. Núria Ramos: biological studies. Miquel Nuez, Jewel Ann Maria Xavier: physicochemical studies. Duane Choquesillo-Lazarte: X-ray structure measurement. Reijo Sillanpää: discussion and writing results of X-ray structures. Francesc Teixidor and Isabel Romero: discussion and writing results of electrochemistry and UV-visible studies. Clara Viñas, Margarita Martinez-Medina: discussions of the research, writing-review and editing. All authors have read and agreed to the submitted version of the manuscript.

Conflicts of interest

The authors declare no competing financial interests.

Acknowledgements

References

1 https://www.who.int/news-room/fact-sheets/detail/antibiotic-resistance.

2 S. S. Magill, J. R. Edwards, W. Bamberg, Z. G. Beldavs, G. Dumyati, M. A. Kainer, R. Lynfield, M. Maloney, L. McAllister-Hollod, J. Nadle, S. M. Ray, D. L. Thompson, L. E. Wilson and S. K. Fridkin, Multistate point-prevalence survey of health care-associated infections. Emerging Infections Program Healthcare-Associated Infections and Antimicrobial Use Prevalence Survey Team, *N. Engl. J. Med.*, 2014, **370**(13), 1198–1208.

3 S. Santajit and N. Indrawattana, Mechanisms of Antimicrobial Resistance in ESKAPE Pathogens, *BioMed Res. Int.*, 2016, 2475067.

4 (a) X. Gu, M. Qiu, H. Sun, J. Zhang, L. Cheng, C. Deng and Z. Zhong, Polytyrosine nanoparticles enable ultra-high loading of doxorubicin and rapid enzyme-responsive drug release, *Biomater. Sci.*, 2018, **6**, 1526–1534; (b) H. Han, Y. Hou, X. Chen, P. Zhang, M. Kang, Q. Jin, J. Ji and M. Gao, Metformin-Induced Stromal Depletion to Enhance the Penetration of Gemcitabine-Loaded Magnetic Nanoparticles for Pancreatic Cancer Targeted Therapy, *J. Am. Chem. Soc.*, 2020, **142**, 4944–4954; (c) Q. Jin, Y. Deng, X. Chen and J. Ji, Rational Design of Cancer Nanomedicine for Simultaneous Stealth Surface and Enhanced Cellular Uptake, *ACS Nano*, 2019, **13**, 954–977; (d) N. Fernandes, C. F. Rodrigues, A. F. Moreira and I. J. Correia, Overview of the application of inorganic nanomaterials in cancer photothermal therapy, *Biomater. Sci.*, 2020, **8**, 2990–3020; (e) Q. Wang, N. Jiang, B. Fu, F. Huang and J. Liu, Self-assembling peptide-based nanodrug delivery systems, *Biomater. Sci.*, 2019, **7**, 4888–4911; (f) Y. Deng, P. Song, X. Chen, Y. Huang, L. Hong, Q. Jin and J. Ji, 3-Bromopyruvate-Conjugated Nanoplatform-Induced Pro-Death Autophagy for Enhanced Photodynamic Therapy against Hypoxic Tumor, *ACS Nano*, 2020, **14**, 9711–9727; (g) D. Sun, S. Zhou and W. Gei, What went wrong with anticancer nanomedicine design and how to make it right, *ACS Nano*, 2020, **14**, 12281–12290.

5 (a) Y. Liu, L. Shi, L. Su, H. C. van der Mei, P. C. Jutte, Y. Ren and H. J. Busscher, Nanotechnology-based antimicrobials and delivery systems for biofilm-infection control, *Chem. Soc. Rev.*, 2019, **48**, 428–446; (b) M. Chai, Y. Gao,

J. Liu, Y. Deng, D. Hu, Q. Jin and J. Ji, Polymyxin B-Polysaccharide Polyion Nanocomplex with Improved Biocompatibility and Unaffected Antibacterial Activity for Acute Lung Infection Management, *Adv. Healthcare Mater.*, 2020, **9**, 1901542, (1 of 8). (*c*) M. A. Hutnick and J. K. Pokorski, *Mol. Pharm.*, 2018, **15**, 2910–2921; (*d*) A. Gupta, S. Mumtaz, C.-H. Li, I. Hussain and V. M. Rotello, Combatting antibiotic-resistant bacteria using nanomaterials, *Chem. Soc. Rev.*, 2019, **48**(2), 415–427.

6 S. Wang, Y. Gao, Q. Jin and J. Ji, Emerging antibacterial nanomedicine for enhanced antibiotic therapy, *Biomater. Sci.*, 2020, **8**, 6825–6839.

7 C. Brown, F. Chen, C. G. Dowson, G. Dujardin, N. Jung, A. P. King, A. M. Mansour, M. Massi, J. Moat, H. A. Mohamed, A. K. Renfrew, P. J. Rutledge, P. J. Sadler, M. H. Todd, C. E. Willans, J. J. Wilson, M. A. Cooper and M. A. T. Blaskovich, Metal complexes as a promising source for new antibiotics, *Chem. Sci.*, 2020, **11**, 2627–2639.

8 A small molecule within the fields of pharmacology and molecular biology is an "organic compound" with a size on the order of 1 nm and a molecular weight <900 daltons that may regulate a biological process.

9 (*a*) *Electron Deficient Boron and Carbon Clusters*, ed. G. A. Olah, K. Wade and R. E. Williams, Wiley-Interscience, 1st edn, 1991; (*b*) C. E. Housecroft, *Boranes and Metalloboranes: Structure, bonding, and reactivity (Ellis Horwood Series in Inorganic Chemistry)*, Pearson Higher Education, 2nd edn, 1994; (*c*) C. E. Housecroft, *Metal-Metal Bonded Carbonyl Dimers and Clusters*, Oxford University Press, 1st edn, 1996.

10 R. N. Grimes, *Carboranes*, Elsevier Inc., New York, 3rd edn, 2016.

11 J. Plesek, Chemistry of deltahedral boron compounds and organic chemistry. Principal similarity and principal difference, *Chem. Rev.*, 1996, **90**(5), 273–279.

12 (*a*) F. Issa, M. Kassiou and L. M. Rendina, Boron in Drug Discovery: Carboranes as Unique Pharmacophores in Biologically Active Compounds, *Chem. Rev.*, 2011, **111**(9), 5701–5722; (*b*) M. Scholz and E. Hey-Hawkins, Carbaboranes as Pharmacophores: Properties, Synthesis, and Application Strategies, *Chem. Rev.*, 2011, **111**(9), 7035–7062; (*c*) Z. J. Leśnikowski, Challenges and Opportunities for the Application of Boron Clusters in Drug Design, *J. Med. Chem.*, 2016, **59**, 7738–7758; (*d*) P. Stockmann, M. Gozzi, R. Kuhnert, M. B. Sárosi and E. Hey-Hawkins, New keys for old locks: carborane-containing drugs as platforms for mechanism-based therapies, *Chem. Soc. Rev.*, 2019, **48**, 3497–3512.

13 J. Poater, C. Vinas, I. Bennour, S. E. Gordils, M. Sola and F. Teixidor, Too Persistent to Give Up: Aromaticity in Boron Clusters Survives Radical Structural Changes, *J. Am. Chem. Soc.*, 2020, **142**(20), 9396–9407.

14 (*a*) J. Rais and P. Selucky, New Trends in the Separation of Cesium, Strontium, and Transplutonides by Extraction Methods, *Nucleon*, 1992, **1**, 17; (*b*) S. D. Reilly, C. F. V. Mason and P. H. Smith, *Cobalt(III) Dicarbollide: A Potential 137Cs and 90Sr Waste Extraction Agent, Report LA-11695*, Los Alamos National Laboratory, Los Alamos, NM, 1990.

15 M. Tarrés, E. Canetta, E. Paul, J. Forbes, K. Azzouni, C. Viñas, F. Teixidor and A. J. Harwood, Biological interaction of living cells with COSAN-based synthetic vesicles, *Sci. Rep.*, 2015, **5**, 7804.

16 I. Fuentes, T. García-Mendiola, S. Sato, M. Pita, H. Nakamura, E. Lorenzo, F. Teixidor, F. Marques and C. Viñas, Metallacarboranes on the Road to Anticancer Therapies: Cellular Uptake, DNA Interaction, and Biological Evaluation of Cobaltabisdicarbollide [COSAN]⁻, *Chem. – Eur. J.*, 2018, **24**, 17239–17254.

17 C. Masalles, S. Borrós, C. Viñas and F. Teixidor, Extraordinary Overoxidation resistance increase in self–doped polypyrroles by using non–conventional low charge-density anions, *Adv. Mater.*, 2002, **14**, 826–829.

18 A. Zaulet, F. Teixidor, P. Bauduin, O. Diat, P. Hirva, A. Ofori and C. Viñas, Deciphering the role of the cation in anionic cobaltabisdicarbollide clusters, *J. Organomet. Chem.*, 2018, **865**, 214–225.

19 D. C. Malaspina, C. Viñas, F. Teixidor and J. Faraudo, Atomistic simulations of COSAN: amphiphiles without a Head-and-Tail design have a "head and tail" surfactant behavior, *Angew. Chem., Int. Ed.*, 2020, **59**, 3088–3092.

20 (*a*) A. M. A. Abdelgawwad, J. A. M. Xavier, D. Roca-Sanjuán, C. Viñas, F. Teixidor and A. Francés-Monerris, Light-Induced On/Off Switching of the Surfactant Character of the o-Cobaltabis(dicarbollide) Anion with No Covalent Bond Alteration, *Angew. Chem., Int. Ed.*, 2021, **60**, 25753–25757; (*b*) P. Matejícek, P. Cígler, K. Prochazka and V. Kral, Molecular assembly of metallacarboranes in water: light scattering and microscopy study, *Langmuir*, 2006, **22**, 575–581; (*c*) P. Bauduin, S. Prevost, P. Farras, F. Teixidor, O. Diat and T. Zemb, A Theta-Shaped Amphiphilic Cobaltabisdicarbollide Anion: Transition From Monolayer Vesicles to Micelles, *Angew. Chem., Int. Ed.*, 2011, **50**, 5298–5300.

21 C. Viñas, M. Tarrés, P. González-Cardoso, P. Farràs, P. Bauduin and F. Teixidor, Surfactant behaviour of metallacarboranes. A study based on the electrolysis of water, *Dalton Trans.*, 2014, **43**, 5062–5068.

22 (*a*) A. I. Stoica, C. Viñas and F. Teixidor, Cobaltabisdicarbollide anion receptor for enantiomer-selective membrane electrodes, *Chem. Commun.*, 2009, **33**, 4988–4990; (*b*) A. I. Stoica, C. Viñas and F. Teixidor, Application of the cobaltabisdicarbollide anion to the development of ion selective PVC membrane electrodes for tuberculosis drug analysis, *Chem. Commun.*, 2008, **48**, 6492–6494.

23 (*a*) I. Fuentes, J. Pujols, C. Viñas, S. Ventura and F. Teixidor, Dual Binding Mode of Metallacarborane Produces a Robust Shield on Proteins, *Chem. – Eur. J.*, 2019, **25**, 12820–12829; (*b*) T. M. Goszczynski, K. Fink, K. Kowalski, Z. J. Lesnikowski and J. Boratynski, Interactions of Boron Clusters and their Derivatives with Serum Albumin, *Sci. Rep.*, 2017, **7**, 9800.

24 C. Verdiá-Báguena, A. Alcaraz, V. M. Aguilella, A. M. Cioran, S. Tachikawa, H. Nakamura, F. Teixidor and C. Viñas, Amphiphilic COSAN and I2-COSAN crossing synthetic lipid membranes: planar bilayers and liposomes, *Chem. Commun.*, 2014, **50**, 6700–6703.

25 (*a*) R. A. Spryshkova, L. I. Karaseva, V. A. Brattsev and N. G. Serebryakov, Toxicity of functional derivatives of polyhedral carboranes, *Med. Radiol.*, 1981, **26**, 62–64; (*b*) R. A. Spryshkova, V. A. Brattsev, T. L. Sherman and V. I. Stanko, Accumulation of carborane compounds in the tissues of some animals during Neutron Capture Therapy, *Med. Radiol.*, 1981, **26**, 51–55.

26 M. Tarrés, E. Canetta, C. Viñas, F. Teixidor and A. J. Harwood, Imaging in living cells using νB–H Raman spectroscopy: monitoring COSAN uptake, *Chem. Commun.*, 2014, **50**, 3370–3372.

27 (*a*) O. N. Kazheva, G. G. Alexandrov, A. V. Kravchenko, V. A. Starodub, I. A. Lobanova, I. B. Sivaev, V. I. Bregadze, L. V. Titov, L. I. Buravov and O. A. Dyachenko, Molecular conductors with 8,8′-diiodo cobalt bis(dicarbollide) anion, *J. Organomet. Chem.*, 2009, **694**, 2336–2342; (*b*) L. I. Zakharkin, V. A. Ol'shevskaya, E. V. Balagurova and P. V. Petrovskii, Palladium-catalyzed cross coupling of the bis(9-iodo-1,2-dicarbollyl)cobaltate anion with organic magnesium and zinc compounds, yielding bis[9-alkyl(aryl)-1,2-dicarbollyl]cobaltate anions, *Russ. J. Gen. Chem.*, 2000, **70**, 550–551; (*c*) O. N. Kazheva, G. G. Aleksandrov, A. V. Kravchenko, V. A. Starodub, G. G. Zhigareva, I. B. Sivaev, V. I. Bregadze, L. I. Buravov, L. V. Titov and O. A. Dyachenko, Synthesis, structures, and conductivities of salts (BEDT-TTF)[9,9 '(12 ')-I-2-3,3 '-Co(1,2-C2B9H10)(2)] and (TTF)[9,9 ',12,12 '-I-4-3,3 '-Co(1,2-C2B9H9)(2)], *Russ. Chem. Bull.*, 2010, **59**, 1137–1144.

28 (*a*) P. K. Hurlburt, R. L. Miller, K. D. Abney, T. M. Foreman, R. J. Butcher and S. A. Kinkhead, New synthetic routes to B-halogenated derivatives of cobalt dicarbollide, *Inorg. Chem.*, 1995, **34**, 5215–5219; (*b*) L. Matel, F. Macasek, P. Rajec, S. Hermanek and J. Plesek, B-Halogen derivatives of the bis(1,2-dicarbollyl)cobalt(III) anion, *Polyhedron*, 1982, **1**, 511–519; (*c*) J. Rais, J. Plesek, P. Selucky, M. Kyrs and L. Kadlecova, Extraction of cesium with derivatives of carborane into nitrobenzene, *J. Radioanal. Nucl. Chem.*, 1991, **148**(2), 349–357; (*d*) P. Selucky, J. Rais, M. Kyrs and L. Kadlecova, Extraction of fission-products with 1,2-dichloroethane solutions of hexabromo derivative of cobalt dicarbollide from nitric-acid medium, *J. Radioanal. Nucl. Chem.*, 1991, **148**(2), 227–233.

29 A. Pepiol, F. Teixidor, R. Sillanpää, M. Lupu and C. Viñas, Stepwise Sequential Redox Potential Modulation Possible on a Single Platform, *Angew. Chem., Int. Ed.*, 2011, **50**, 12491–12495.

30 R. Nuñez, I. Romero, F. Teixidor and C. Viñas, Icosahedral boron clusters: a perfect tool for the enhancement of polymer features, *Chem. Soc. Rev.*, 2016, **45**, 5147–5173.

31 M. Navascuez, D. Dupin, H.-J. Grand, V. Gómez-Vallejo, I. Loinaz, U. Cosido and J. Llop, COSAN-stabilised omega-3 oil-in-water nanoemulsions to prolong lung residence time for poorly water soluble drugs, *Chem. Commun.*, 2020, **56**, 8972–8975.

32 K. Fin and M. Uchman, Boron cluster compounds as new chemical leads for antimicrobial Therapy, *Coord. Chem. Rev.*, 2021, **431**, 213684.

33 M. J. Macielag, *Chemical properties of antibacterials and their uniqueness in Antibiotic Discovery and Development*, ed. T. J. Dougherty and M. J. Pucci, Springer US, 2012, pp. 801–802.

34 C. Viñas, F. Teixidor and A. J. Harwood, Cobaltabisdicarbollide-based synthetic vesicles: From biological interaction to in vivo imaging, in *Boron-Based Compounds: Potential and Emerging Applications in Medicine*, ed. E. Hey-Hawkins and C. Viñas, John Wiley & Sons, 2018, ch. 2.2, pp. 150–171.

35 (*a*) M. F. Hawthorne, D. C. Young and P. A. Wegner, Carbametallic boron hydride derivatives. I. Apparent analogs of ferrocene and ferricinium ion, *J. Am. Chem. Soc.*, 1965, **87**, 1818–1819; (*b*) M. F. Hawthorne and T. D. Andrews, Carborane analogues of cobalticinium ion, *J. Chem. Soc., Chem. Commun.*, 1965, 443–444; (*c*) M. F. Hawthorne, D. C. Young, T. D. Andrews, D. V. Howe, R. L. Pilling, A. D. Pitts, M. Reintjes, L. F. Warren Jr. and P. A. Wegner, pi.-Dicarbollyl derivatives of the transition metals. Metallocene analogs, *J. Am. Chem. Soc.*, 1968, **90**, 879–896; (*d*) C. Viñas, J. Pedrajas, J. Bertran, F. Teixidor, R. Kivekäs and R. Sillanpää, Synthesis of Cobaltabis(dicarbollyl) Complexes Incorporating Exocluster SR Substituents and the Improved Synthesis of [3,3′-Co(1-R-2-R'-1,2-C2B9H9)2]- Derivatives, *Inorg. Chem.*, 1997, **36**, 2482–2486; (*e*) I. Bennour, A. Cioran, F. Teixidor and C. Viñas, 3,2,1 and stop! An innovative, straightforward and clean route for the flash synthesis of metallacarboranes, *Green Chem.*, 2019, **21**, 1925–1928.

36 T. I. Rokitskaya, I. D. Kosenko, I. B. Sivaev, Y. N. Antonenko and V. I. Bregadze, Fast flip–flop of halogenated cobalt bis(dicarbollide) anion in a lipid bilayer membrane, *Phys. Chem. Chem. Phys.*, 2017, **19**, 25122–25128.

37 T. Garcia-Mendiola, V. Bayon-Pizarro, A. Zaulet, I. Fuentes, F. Pariente, F. Teixidor, C. Viñas and E. Lorenzo, Metallacarboranes as tunable redox potential electrochemical indicators for screening of gene mutation, *Chem. Sci.*, 2016, **7**, 5786–5797.

38 J. Brus, A. Zhigunov, J. Czernek, L. Kobera, M. Uchman and P. Matejicek, Control over the Self-Assembly and Dynamics of Metallacarborane Nanorotors by the Nature of the Polymer Matrix: A Solid-State NMR Study, *Macromolecules*, 2014, **47**, 6343–6354.

39 O. N. Kazheva, A. V. Kravchenko, I. D. Kosenko, G. G. Alexandrov, D. M. Chudak, V. A. Starodub, I. A. Lobanova, V. I. Bregadze, L. I. Buravov, S. G. Protasova and O. A. Dyachenko, *J. Organomet. Chem.*, 2017, **849–850**, 261–267.

40 (*a*) CSD consulted in March 15th 2021. (*b*) F. H. Allen, The Cambridge Structural Database: a quarter of a million

crystal structures and rising, *Acta Crystallogr., Sect. B: Struct. Sci.*, 2002, **58**, 380–388; (*c*) I. J. Bruno, J. C. Cole, P. R. Edgington, M. Kessler, C. F. Macrae, P. McCabe, J. Pearson and R. Taylor, New software for searching the Cambridge Structural Database and visualizing crystal structures, *Acta Crystallogr., Sect. B: Struct. Sci.*, 2002, **58**, 389–397.

41 D. M. P. Mingos and A. L. Rohl, Size and shape characteristics of inorganic molecules and ions and their relevance to molecular packing problems, *J. Chem. Soc., Dalton Trans.*, 1991, 3419–3425.

42 P. Sivy, A. Preisinger, O. Baumgartner, F. Valach, B. Koren and L. Matel, Structure of caesium 3,3′-commo-bis(8,9,12-tribromooctahydro-1,2-dicarba-3-cobalta-closo-dodecaborate) (1-), *Acta Crystallogr., Sect. C: Cryst. Struct. Commun.*, 1986, **42**, 24–27.

43 (*a*) G. Chevrot, R. Schurhammer and G. Wipff, Surfactant Behavior of "Ellipsoidal" Dicarbollide Anions: A Molecular Dynamics Study, *J. Phys. Chem. B*, 2006, **110**, 9488–9498.

44 M. Nuez-Martinez, C. I. G. Pinto, J. F. Guerreiro, F. Mendes, F. Marques, A. Muñoz-Juan, J. A.-M. Xavier, A. Laromaine, V. Bitonto, N. Protti, S. Geninatti Crich, F. Teixidor and C. Viñas, Cobaltabis(dicarbollide) ([o-COSAN]−) as Multifunctional Chemotherapeutics: A Prospective Application in Boron Neutron Capture Therapy (BNCT) for Glioblastoma, *Cancers*, 2021, **13**, 6367.

45 M. Corsini, F. Fabrizi de Biani and P. Zanello, Mononuclear metallacarboranes of groups 6–10 metals: Analogues of metallocenes: Electrochemical and X-ray structural aspects, *Coord. Chem. Rev.*, 2006, **250**, 1351–1372.

46 M. Lupu, A. Zaulet, F. Teixidor, E. Ruiz and C. Viñas, Negatively Charged Metallacarborane Redox Couples with Both Members Stable to Air, *Chem. – Eur. J.*, 2015, **21**(18), 6888–6897.

47 I. Guerrero, Z. Kelemen, C. Viñas, I. Romero and F. Teixidor, Metallacarboranes as Photoredox Catalysts in Water, *Chem. – Eur. J.*, 2020, **26**, 5027–5036.

48 (*a*) C. A. Lipinski, F. Lombardo, B. W. Dominy and P. J. Feeney, Experimental and computational approaches to estimate solubility and permeability in drug discovery and development settings, *Adv. Drug Delivery Rev.*, 2001, **46**, 3–26; (*b*) W. L. Jorgensen and E. M. Duffy, Prediction of drug solubility from structure, *Adv. Drug Delivery Rev.*, 2002, **54**, 355–366; (*c*) J. Wang, G. Krudy, T. Hou, W. Zhang, G. Holland and X. Xu, Development of reliable aqueous solubility models and their application in druglike analysis, *J. Chem. Inf. Model*, 2007, **47**, 1395–1404.

49 O. N. Kazheva, G. G. Alexandrov, A. V. Kravchenko, I. B. Sivaev, I. D. Kosenko, I. A. Lobanova, M. Kajnakova, L. I. Buravov, V. I. Bregadze, A. Feher, V. A. V. Starodub and O. A. Dyachenko, Synthesis, structure, electrical and magnetic properties of (BEDT-TTF)$_2$[3,3′-Fe(1,2-C$_2$B$_9$H$_{11}$)$_2$], *Inorg. Chem. Commun.*, 2012, **15**, 106–108.

50 The size was measured from a search at the Cambridge Structural Database (CSD) done on January 19th 2022.

51 The Partition Coefficient (P) is defined as the ratio of the amount of compound present in the organic phase (*n*-octanol) to the amount present in the aqueous phase.

52 V. W. Pike, PET radiotracers: crossing the blood–brain barrier and surviving metabolism, *Trends Pharmacol. Sci.*, 2009, **30**, 431–440.

53 (*a*) T. Popova, A. Zaulet, F. Teixidor, R. Alexandrova and C. Viñas, Investigations on antimicrobial activity of cobaltabisdicarbollides, *J. Organomet. Chem.*, 2013, **747**, 229–234; (*b*) Y. Zheng, W. W. Liu, Y. Chen, H. Jiang, H. Yan, I. Kosenko, L. Chekulaeva, I. Sivaev, V. Bregadze and X. M. Wang, A Highly potent antibacterial agent targeting methicillin-resistant staphylococcus aureus based on cobalt bis(1,2-dicarbollide) alkoxy derivative, *Organometallics*, 2017, **36**(18), 3484–3490; (*c*) E. Kvasničková, J. Masák, J. Čejka, O. Matátková and V. Šícha, Preparation, characterization, and the selective antimicrobial activity of N-alkylammonium 8-diethyleneglycol cobalt bis-dicarbollide derivatives, *J. Organomet. Chem.*, 2017, **827**, 23–31.

54 I. Romero, M. Martinez-Medina, C. Camprubí-Font, I. Bennour, D. Moreno, L. Martínez-Martínez, F. Teixidor, M. A. Fox and C. Viñas, Metallacarborane Assemblies as Effective Antimicrobial Agents, Including a Highly Potent Anti-MRSA Agent, *Organometallics*, 2020, **39**, 4253–4264.

55 D. Brusselle, P. Bauduin, L. Girard, A. Zaulet, C. Viñas, F. Teixidor, I. Ly and O. Diat, Lyotropic Lamellar Phase Formed from Monolayered θ-Shaped Carborane-Cage Amphiphiles, *Angew. Chem., Int. Ed.*, 2013, **52**, 12114–12118.

56 A. Ebbensgaard, H. Mordhorst, F. M. Aarestrup and E. B. Hansen, The Role of Outer Membrane Proteins and Lipopolysaccharides for the Sensitivity of Escherichia coli to Antimicrobial Peptides, *Front. Microbiol.*, 2018, **9**, 2153.

57 M. Vaara, Agents that increase the permeability of the outer membrane, *Microbiol. Rev.*, 1992, 395–411.

58 DOI: **10.1016/j.bbrep.2016.03.014**.

59 DOI: **10.1016/bs.podrm.2020.07.005**.

60 I. Bennour, M. Haukka, F. Teixidor, C. Viñas and A. Kabadou, Crystal structure and Hirshfeld surface analysis of [N(CH$_3$)$_4$][2,2′-Fe(1,7-closo-C$_2$B$_9$H$_{11}$)$_2$], *J. Organomet. Chem.*, 2017, **846**, 74–80.

61 The chemical shifts of the Boron vertices were assigned according to: A. M. Cioran, F. Teixidor and C. Viñas, The effect of a paramagnetic metal ion within a molecule: comparison of the structurally identical paramagnetic [3,3-Fe (1,2-C2B9H11)2]− with the diamagnetic [3,3-Co(1,2-C$_2$B$_9$H$_{11}$)$_2$]− sandwich complexes, *Dalton Trans.*, 2015, **44**, 2809–2818.

62 G. M. Sheldrick, A short history of SHELX, *Acta Crystallogr., Sect. A: Found. Crystallogr.*, 2008, **64**(1), 112–122.

63 *Bruker APEX3 Software, V2019.0-1*, Bruker AXS Inc., Madison, Wisconsin, 2019.

64 L. Krause, R. Herbst-Irmer, G. M. Sheldrick and D. Stalke, *J. Appl. Crystallogr.*, 2015, **48**, 3–10.

65 O. V. Dolomanov, L. J. Bourhis, R. J. Gildea, J. A. K. Howard and H. Puschmann, *J. Appl. Crystallogr.*, 2009, **42**, 339–341.

66 International Standards Organisation, *Clinical laboratory testing and in vitro diagnostic test systems d Susceptibility testing of infectious agents and evaluation of performance of antimicrobial susceptibility test devices. Part 1: Reference method for testing the in vitro activity of antimicrobial agents against rapidly growing aerobic bacteria involved in infectious diseases. ISO-20776e1*, 2006.

67 CLSI, *Methods for Determining Bactericidal Activity of Antimicrobial Agents; Approved Guideline. document M26-A*, 1999.

68 R. Hamoud, S. Zimmermann, J. Reichling and M. Wink, Synergistic interactions in two-drug and three-drug combinations (thymol, EDTA and vancomycin) against multi drug resistant bacteria including E. coli, *Phytomedicine*, 2014, **21**(4), 443–447.

69 DOI: **10.1016/j.phymed.2013.10.016**.